NAG1-11

DRA

TEXAS A&M UNIVERSITY
MECHANICAL ENGINEERING DEPARTMENT
COLLEGE STATION, TEXAS 77843-3123

A Final Report

entitled

ANALYTICAL STUDY OF TWIN-JET SHIELDING

NASA Grant No. NAG 1-11

Submitted by the

TEXAS A&M RESEARCH FOUNDATION

to

National Aeronautics and Space Administration
Langley Research Center

Prepared by

Dr. Carl H. Gerhold

of the

Department of Mechanical Engineering
Texas A&M University
College Station, Texas 77843

December, 1983

TABLE OF CONTENTS

PAGE

I. SUMMARY 1

II. INTRODUCTION 3

III. MODEL DEVELOPMENT 5
1. Formulation of the Model 5
2. Solution of the Model 7

IV. PARAMETER STUDY 12
1.. Identification of Shielding Zones 12
1.1 Transmission Dominant Zone 14
1.1.1 Location of Minimum Sound Pressure 14
1.1.2 Transmission Zone Cut-off 15
1.2 Transition Zone 16
1.3 Diffraction Dominant Zone 17
1.3.1 Diffraction Zone Cut-off 17
2. Effect of Jet Operation Parameters 17
2.1 Mach Number 18
2.1.1 Transmission Dominant Zone 18
2.1.2 Diffraction Dominant Zone 18
2.2.1 Transmission Dominant Zone 19
2.2.2 Diffraction Dominant Zone 19

V. MODIFIED JET SOURCE MODEL 22
1. Description of the Jet Noise Model 22
1.1 Basic Directivity Model 23
1.2 Spectral Amplitude Functions 24
2. Comparison to Heat Jet Spectra 28

VI. MODIFIED SHIELDING JET MODEL 30
1. Development of Model 31
1.1 Spreading Parameter 32
1.2 Velocity Representation 33
1.2.1 Centerline Velocity Approximation 33
1.2.2 Velocity Profiles 34
1.2.3 Slug Flow Approximation 35
2. Comparision to Experiment 36
2.1 Isothermal Jet, M = 0.531 36
2.2 Isothermal Jet, M = 0.886 37
2.3 Simulated Hot Jet 37

VII. ESTIMATE OF TWIN-JET SHIELDING 40

Analytical Study of Twin-Jet Shielding

I. SUMMARY

This report summarizes the development of the analytical model of twin-jet shielding. The models consist of a point noise source impinging on a cylinder of heated flow in which the temperature and flow velocity are uniform across the cross-section.

In the formulation of the model, the wave equations are written for the regions outside the flow and within the flow cylinder. The solutions to the wave equations are matched at the jet boundary under the conditions of continuity of pressure and continuity of the vortex sheet. The solution reduces to an indefinite integral involving Bessel functions. The integral is solved approximately using a saddle point method.

The resulting model is analysed in order to identify the mechanisms of transmission and diffraction which control shielding in the shadow of the shielding jet. The impact that variations in jet operating parameters has on shielding is investigated. It is found that in the zone of the shadow region in which transmission dominates, shielding is relatively insensitive to variations of such parameters as Mach Number and spacing ratio.

In the zone in which diffraction dominates, shielding is more sensitive to variations in Mach Number, jet temperature and spacing ratio.

The basic model is modified in order to represent more accurately both the noise emission of a jet noise source and the widening of the shielding jet.

The modified noise source model is developed in order that the sound level due to the jet noise at a far field receiver can be estimated. The model consists of a point noise source with a directivity function super-imposed. The function simulates both the spatial and frequency dependent characteristics of the jet.

The shielding jet model consists of two parts; the jet widening and the decreasing velocity downstream of the jet exit. The jet is assumed to spread linearly, with a Mach Number dependent widening. Corresponding to the widening is a decrease in flow velocity from which an equivalent slug flow velocity is approximated. The shielding analysis with the modified jet is found to improve the estimated shielding of a point noise source in the far downstream region of the jet.

The model is compared to experimental data for jet-by-jet shielding. The influence of the shielding jet as a secondary noise source is characterized by estimating the reflection of the shielding jet noise by the source jet. While other sound rays reach the receiver after multiple reflections between the jets, this first reflection is the only one considered in simulating the jet-by-jet shielding. The comparisons to experiment shows generally favorable agreement in the far downstream region, except that the estimated attenuations shows more oscillatory behavior than the measured. In the near downstream regions, the model shows trends characteristic of the transmission dominant zone, while the experiment is much smoother. This indicates that the higher order reflections of sound between the jets are more significant in the near downstream region.

II. INTRODUCTION

One of the drawbacks of the growing dependence on air travel is the increased impact of aircraft noise. Assessment and reduction of this impact requires identification of aircraft generated noise levels. To this end, the Noise Technology Branch of NASA/Aircraft Noise Reduction Division is developing and refining an aircraft noise prediction computer program. Noise estimation includes consideration not only of noise sources on the aircraft, but also of the propagation path between source and receiver. One of the numerous factors affecting the noise transmission path is shielding of one jet by another. The shielding jet, because of the high temperature and flow speed with respect to the immediate surroundings, acts as a partial barrier between the source and the receiver. The resultant noise reduction not only affects the overall aircraft noise level, but also indicates the possibility of jet engine installation as a means of aircraft noise control.

It is the purpose of this project to develop an analytical method to estimate the shielding of one jet by an adjacent jet in a twin jet configuration.

The problem of reflection and transmission of sound by a moving medium has been addressed assuming a plane wave incident on a plane interface (1,2,3,4). Ray tracing techniques have been applied to two-dimensional jets (5) and cold jets (6).

In this study, the three-dimensional case is considered. The model developed consists of the sound field emitted from a stationary, discrete frequency point source, which impinges on a cylinder of

locally parallel flow. The temperature and velocity profiles are uniform in the jet at any location down stream of the nozzle.

The wave equations are written for the acoustic velocity potential in the region outside the jet and in the region within the jet. The equations incorporate the convective effect due to local mean flow. The velocity potentials in the two regions are matched at the flow boundary by the conditions of pressure continuity and continuity of the vortex sheet.

The solution for the acoustic pressure in the far field, which is derived from the velocity potential, is normalized by the incident acoustic pressure. This incident sound pressure is the sound pressure at the same location in the far field in the absence of the jet. This normalized sound pressure is related to the directivity.

The model is used to evaluate the effect on the far field noise radiation due to variations of such operating parameters as shielding jet flow speed and temperature, and the spacing between the source and the shielding jet.

Comparison of the model to experimental jet shielding data has necessitated modifications to improve the accuracy of the estimated sound level at the far-field receiver location. These modifications include a jet noise source model which simulates the noise emission of a real jet, and incorporation of jet widening in the shielding jet.

III. MODEL DEVELOPMENT

1. Formulation of the Model

The mechanisms by which shielding occurs are reflection and refraction of sound at the boundary between the jet and the surrounding air and by diffraction around the jet.

The noise source is modelled by a stationary, discret frequency point source located at (r_o, θ_o, o). The shielding jet is a cylinder of radius a, and is infinite in extent along the z-axis. The temperature and flow velocity are uniform across the cylinder cross-section. The model is illustrated in Figure 1. The expression for acoustic velocity potential is written for two regions; region I is outside the jet, region II is within the jet.

In region 1 (outside the flow-incident upon the shielding jet)

$$\nabla^2\phi - \frac{1}{c_o^2}\phi_{tt} = Q_o e^{-i\omega t}\,\delta(r-r_o)\,\delta(\theta-\theta_o)\,\delta(z) \qquad 1a)$$

In region I (outside the flow-reflected from the shielding jet)

$$\nabla^2\phi - \frac{1}{c_o^2}\phi_{tt} = o \qquad 1b)$$

In region II (inside the flow)

$$\nabla^2\phi - M^2\phi_{zz} - \frac{2M}{c_1}\phi_{zt} - \frac{1}{c_1^2}\phi_{tt} = o \qquad 2)$$

Where:

(r_o, θ_o, o) - location of point source

(r, θ, z) - location of the receiver

ω - source frequency

Q_o - source strength

c - sound speed

M - mach number - (jet flow speed/c)

$$\nabla^2\phi = \phi_{rr} + \frac{1}{r}\ \phi_r + \frac{1}{r^2}\phi_{\theta\theta} + \phi_{zz}$$

Note: The subscript o refers to conditions outside the flow (ambient), 1 refers to conditions within the heated jet.

The boundary conditions at the interface between the ambient air and the jet are:

1) Pressure continuity

$$(p)_o = (p)_1 \quad \text{at } r = a$$

or-

$$-\rho_o(\phi_t)_o = -\rho_1(\phi_t + V\phi_z)_1 \quad \text{at } r = a \qquad 3)$$

2) Continuity of the vortex sheet (1,2). This condition states that the displacement of the medium is continuous and symmetrical at the boundary; r = a. Denoting this displacement by $\eta = (z,t)$, then:

$$\left.\frac{D\eta}{Dt}\right|_o = \left.\frac{D\eta}{Dt}\right|_1 \quad \text{at } r = a$$

or-

$$(\eta_t)_o = (\eta_t + V\eta_z)_1, \quad \text{at } r = a \qquad 4)$$

Time is eliminated from equations 1 and 2 by assuming:

$$\phi(r, \theta, z, t) = \psi(r, \theta, z)e^{-i\omega t}$$

The problem is reduced to a two-dimensional formulation by the Fourier transform:

$$\tilde{\psi} = \frac{1}{2\pi}\int_{-\infty}^{+\infty} \psi e^{-ik_z z}\, dz$$

with corresponding inverse:

Solution of the transformed equations, irclusion of the boundary conditions and inverse transformations yields the equation for the

acoustic velocity potential in the far field ((r>>a):

$$\phi = \frac{-iQ_o e^{-i\omega t}}{8\pi} \sum_{m=o}^{\infty} \varepsilon_m \cos m(\theta-\theta_o) \int_{-\infty}^{+\infty} H_m(K_o r)\, F_m(K_o,K_1) e^{ik_z(z)}\, dk_z \qquad 5)$$

where:

$$F_m(K_o,K_1) = J_m(K_o r) - \frac{H_m(K_o r_o)\,[J_m(K_1 a)J_m'(K_o a) - TJ_m(K_o a)J_m'(K_1 a)]}{TH_m(K_o a)J_m'(K_1 a) - J_m(K_1 a)H_m'(K_o a)]}$$

$$T = \frac{k_o^2\, c_o^2\, \rho_o k_1}{k_1^2\, c_1^2\, \rho_1 K_o}$$

$$k_o = \omega/c_o$$

$$k_1 = \left(\frac{\omega}{c_1} - Mk_z\right)$$

$$K_o = [k_o^2 - k_z^2]^{1/2},$$

$$K_1 = [k_1^2 - k_z^2]^{1/2}$$

2. Solution of the Model

An approximate solution of the integral in equation 5 is obtained using the Method of Stationary Phase (7). By this method, the solution of the integral I_z, of the form:

$$I_z = \int_{-\infty}^{+\infty} g(\alpha) e^{iz(h(\alpha))} d\alpha \quad \text{as } z \to \infty \qquad 6)$$

is:

$$I_z = \left[\frac{2\pi}{z\,|h''(\alpha_o)|}\right]^{1/2} g(\alpha_o)\; e^{i(z(h(\alpha_o)) \pm \pi/4)} \qquad 7)$$

where:

1) solves $h'(\alpha) = o$

2) the sign in the exponential term goes as the sign of $h''(t_o)$

In order to solve equation 5 in the manner prescribed by equation 6, the following transformations are made.

Let:

$$\alpha = \sqrt{1 - \left(\frac{k_z}{k_o}\right)^2}$$

then:

$$1)\quad dk_z = -\frac{k_o \alpha\, d\alpha}{\sqrt{1-\alpha^2}}$$

$$2)\quad k_1 = \frac{\omega}{c_1} - Mk_z = k_o\left(\frac{c_o}{c_1} - M\sqrt{1-\alpha^2}\right)$$

$$3)\quad K_o = [k_o^2 - k_z^2]^{1/2} = k_o\alpha$$

$$4)\quad K_1 = [k_1^2 - k_z^2]^{1/2} = k_o\left[\left(\frac{c_o}{c_1} - M\sqrt{1-\alpha^2}\right)^2 - 1 + \alpha^2\right]^{1/2}$$

the integral in equation 5:

$$I = \int_{-\infty}^{+\infty} e^{ik_z z} H_m(k_o r)\, F_m(k_{o_1} k_1)\, dk_z$$

becomes:

$$I = -k_o \int_{-\infty}^{+\infty} \frac{\alpha e^{ik_o z\sqrt{1-\alpha^2}}}{\sqrt{1-\alpha^2}} H_m(k_o r\alpha)\, F_m(\alpha)\, d\alpha \qquad 8)$$

In the acoustic far field, r>>1. Assuming that $k_z << k_o$, the argument of the Hankel function becomes large:

$$k_o r\alpha >> 1$$

and the Hankel function is approximated by:

$$H_m(k_o r\alpha) \approx \sqrt{\frac{2}{\pi k_o r\alpha}}\, e^{i(k_o r\alpha - \frac{\pi}{2}(m + 1/2))} \qquad 9)$$

from figure 1, it is seen that:

$$r = R\cos\beta \text{ and } z = R\sin\beta$$

where:

R = distance from origin of the coordinate system to the receiver

$$I = \frac{2i}{R} e^{-im\pi/2} e^{ik_o R} F_m(\cos\beta) \qquad 12)$$

From which the expression for the far field acoustic velocity potential is evaluated:

$$\phi = \frac{Q_o e^{-i\omega t}}{4\pi R} \sum_{m=o}^{\infty} \varepsilon_m \cos m(\theta-\theta_o) e^{\frac{-im\pi}{2}} e^{ik_o R} F_m(\cos\beta) \qquad 13)$$

Where:

$$F_m(\cos\beta) = J_m(k_o r_o \cos\beta) -$$

$$\Big\{ H_m(k_o r_o \cos\beta) \Big[\rho_1 c_1^2 T_1^2 \cos\beta J_m(k_o a T_2) J_m'(k_o a \cos\beta)$$

$$- \rho_o c_o^2 T_2 J_m(k_o a \cos\beta) J_m'(k_o a T_2) \Big] \Big/$$

$$\Big[\rho_1 c_1^2 T_1^2 \cos\beta J_m(k_o a T_2) H_m'(k_o a \cos\beta) - \rho_o c_o^2 T_2 H_m(k_o a \cos\beta) J_m'(k_o a T_2) \Big] \Big\} \qquad 14)$$

where:

$$T_1 = \frac{c_o}{c_1} - M \sin\beta$$

$$T_2 = \left[\left(\frac{c_o}{c_1} - M \sin\beta \right)^2 - \sin^2\beta \right]^{1/2}$$

The total acoustic velocity potential in the far field consists of two parts:

1. The velocity potential of the incident wave:

$$\phi_{in} = \frac{Q_o e^{-i\omega t}}{4\pi R} \sum_{m=o}^{\infty} \varepsilon_m \cos m(\theta-\theta_o) e^{\frac{-im\pi}{2}} e^{ik_o R} J_m(k_o r_o \cos\beta) \qquad 15)$$

2. The velocity potential of the scattered wave:

$$\phi_{sc} = \frac{Q_o e^{-i\omega t}}{4\pi R} \sum_{m=o}^{\infty} \varepsilon_m \cos m(\theta\ \theta_o) e^{\frac{im\pi}{2}} e^{ik_o R} X$$

$$\left\{\text{terms in equation 14) within brackets}\right\} \qquad 16)$$

As a check; when $r_o = o$ (source is located at the origin), the velocity potential of the incident wave reduces to:

$$\phi_{in} = \frac{Q_o e^{ik_o(R-ct)}}{4\pi R}$$

since;

$$J_m(o) = \begin{cases} 1 & m = o \\ o & m \neq o \end{cases}$$

This is the expression for the velocity potential in the far field for radiation from a point source of strength, Q_o, located at the origin of the coordinate system.

IV. PARAMETER STUDY

The total sound pressure is evaluated from the acoustic velocity potential by:

$$P_T = -\rho_o \frac{\partial}{\partial t} \phi_T$$

The incident sound pressure is evaluated from equation 15:

$$P_{in} = -\rho_o \frac{\partial \Phi_{in}}{\partial t} = + \frac{i\omega \bar{Q}_o}{4\pi R} \rho_o \sum_{m=0}^{\infty} \epsilon_m \cos m(\Theta-\Theta) e^{\frac{-im\pi}{2}} e^{ik_o R} J_m(k_o r_o \cos \beta) \qquad 17)$$

The normalized sound pressure is formed from the magnitude of the ratio of the total sound pressure to the incident sound pressure. This normalized sound pressure is a measure of the influence of the shielding jet on the noise source directionality. A value of normalized sound pressure less than one indicates noise reduction; and a value of normalized sound pressure greater than one indicates amplification.

In order to differentiate among the mechanisms of shielding, the normalized sound pressure is evaluated at low frequencies under the following operating conditions.

a) V_1 = Jet velocity = 1552 feet/sec

b) T_1 = Jet temperature = $1238^{\circ}R$

c) T_o = Ambient temperature = $530^{\circ}R$

d) S/D = Spacing parameter = ratio of distance from source to center of jet and jet diameter = 2.67

1. Identification of Shielding Zones

The normalized sound pressure is evaluated in the shielded zone of the jet, for $\theta=\pi$. The contours of normalized sound pressure for $80^{\circ} > \beta > 0$ are plotted against the nondimensional frequency parameter,

$k_o a$, where

$$k_o a = \frac{\omega}{a_o} a$$

and shown in figure 2.

The receiver is directly opposite the jet from the source at $\beta = 0^\circ$ At low frequency, the normalized sound pressure approaches 1.0, indicating that the jet has no effect on the incident sound. As the receiver moves downstream from $\beta = 0^\circ$, the effect is to shift the contours toward lower frequency. For $\beta < 20^\circ$, the contours have a similar form in which the normalized sound pressure decreases rapidly from 1.0 with increasing frequency, until a minimum sound pressure is reached. At higher frequencies, the sound pressure becomes oscillatory.

As $\beta > 20^\circ$, the shift toward lower frequency becomes greater with increasing angle. The contours become smoother, and approach a minimum sound pressure at high frequency asymptotically. The trend continues to $\beta = 46.66^\circ$. At this angle, the normalized sound pressure is a minimum; and is approximately constant over the frequency range of $0.1 < k_o a < 5.0$.

At locations further downstream of $\beta = 46.66^\circ$, the trend reverses, with the contours shifting toward higher frequency as the jet axis is approached.

The locations downstream of the source on the shadow zone side of the shielding jet can be ordered into zones. These zones are characterized by the shape of the normalized sound pressure contours and identified in terms of the shielding mechanism.

1.1 Transmission Dominant Zone

For the range of angles, $0<\beta<20.15^{o}$, the effect of the jet is to scatter the incident sound in the forward direction, that is into the azimuthal half plane, $\pi/2<0<3\pi/2$. The sound incident on the jet is refracted as it transmits through the jet, and little back scattering occurs; as is shown in Figure 3.

Figure 3 shows the azimuthal variation of normalized sound pressure at $\beta=0$ plotted for values of frequency corresponding to $k_o a=$ 1.0, and 5.0. At $k_o a = 1.0$, the wave length of the incident sound is greater than the diameter of the jet. Sound is transmitted through the jet as well as diffracted around the jet. The azimuthal distribution is distorted by this diffraction. As the ratio of wave length to jet diameter becomes less than 1, the refraction of sound as it passes through jet becomes more pronounced. At $k_o a = 5.0$, the sound pressure forms into lobes in the forward direction. The relative uniformity of sound pressure in the backward direction indicates that no reflection back toward the source occurs.

1.1.1 Location of Minimum Sound Pressure

The oscillatory nature of the normalized sound pressure at higher frequencies, shown in figure 2, arises from the standing wave pattern within the shielding jet. The sound wave incident on the cylinder is refracted, not only by the temperature difference between the jet and the surroundings; but also by the difference in flow speed. A sound ray incident on the jet at angle β is refracted according to the relationship [4].

$$\sin \beta_1 = \frac{(1+M)}{c_o/c_1} \sin \beta \qquad (18)$$

This in Snell's Law refraction index modified by convection

effect due to the mean flow. When an acoustic wave is transmitted through a heated layer of thickness, D, the sound power transmission is a minimum at [8]:

$$\alpha_{T_{min}} \quad @ \; k_1 PL = \frac{(2n-1)}{2} \; \pi$$

The sound power transmission is a maximum at:

$$\alpha_{T_{max}} \quad @ \; k_1 PL = n\pi$$

where:

$$k_1 = \frac{\omega}{c_1} = \frac{c_o}{c_1} \; k_o$$

PL = path length through the jet. = $D/\cos\beta_1$

The first minimum does not occur until the incident wave is entrained in the jet, that is, until the incident wavelength is less than the jet diameter. That is satisfied by the condition $k_o a > \pi$. Thus, the lowest sound pressure is expected to occur at:

$$\frac{c_o}{c_1} \; k_o PL = \frac{3\pi}{2} \rightarrow k_o a \approx \frac{3}{4} \; \frac{c_1}{c_o} \; \cos \beta_1 \qquad (19)$$

The expected and observed (from figure 2) locations of minimum are:

β	0°	10°	20°
$k_o a$ (eq. (4))	3.6	3.1	1.4
$k_o a$ (figure 2)	3.6	2.7	1.8

Thus, the simplified relationship of equation (4) estimates the approximate location of the sound pressure minimum in the transmission dominant zone.

1.1.2 Transmission Zone Cut-Off

At the condition:

$$\sin \beta_T = \frac{c_o / c_1}{1 + M} \qquad (20)$$

the refraction angle, β_1, in equation 3, equals 90^o. That is, the refracted wave is directed downstream parallel to the jet axis and transmission through the jet is cut-off. This cut-off angle, shown in previous work by Yeh [4], is also the angle at which the parameter T_2 goes to zero in equation (14), for the total sound pressure. At $T_2 = 0$, the term F_m in the scattered sound pressure, equation (14), reduces to:

$$F_m(\cos\beta) = H_m(k_o S \cos\beta) \frac{J'_m (k_o a \cos\beta)}{H'_m (k_o a \cos\beta)}$$

This expression corresponds to the solution for a point source radiation impinging upon an acoustically hard cylinder [9]. Such a cylinder is one for which the sum of the incident and outgoing scattered radial velocities equal zero.

The transmission zone cut-off angle for the jet considered is calculated to be:

$$\beta_T = 20.15^o$$

While sound transmission does not cease entirely, the decreasing influence of soud transmission through the jet is evidenced in figure 2, for $\beta > 20^o$. The rate of decrease in sound pressure is greater for $\beta < 20^o$. The high frequency oscillation characteristic of the transmitted wave standing wave pattern decreases.

1.2 Transition Zone

It is seen from figure 2 that the normalized sound pressure decreases as β increases beyond β_T, until a minimum value is reached at $\beta = 46.66^o$.

Within this range of angles, the influence of sound transmission

is decreasing; while diffraction of sound around the jet is increasing.

1.3 Diffraction Dominant Zone

As the receiver moves downstream, $\beta > 46.66^{\circ}$ and approaches the jet axis, the normalized sound pressure shifts toward higher frequency. As the angle increases, the line of sight distance from the source to the jet becomes greater. From barrier theory arguments, the expected result of increasing the spacing between the source and the jet is to decrease the attenuation of the lower frequency sounds. This trend is shown in figure 2. Thus, the jet behaves as a barrier in this region and diffraction dominates.

1.3.1 Diffraction Zone Cut-off

At the condition:

$$\sin \beta_D = \frac{c_o/c_1}{M} \tag{21}$$

the parameter T_1 goes to zero in equation (14), and the term, F_m, for the scattered wave reduces to:

$$F_m(\cos\beta) = H_m(k_o S \cos\beta) \frac{J_m(k_o a \cos\beta)}{H_m(k_o a \cos\beta)}$$

This corresponds to the condition of a point source impinging on an acoustically soft cylinder [9], for which the boundary condition at the surface is that the excess pressure equals zero.

It is seen from equation (21) that β_D can exist only for $V_1/c_o \geq 1$ The diffraction zone cut-off angle for the jet considered is calculated from equation (21) to be:

$$\beta_D = 46.66^{\circ}$$

The sound pressure at β_D is relatively invariant over the frequency range shown in figure 2.

2. Effect of Jet Operation Parameters

2.1 Mach Number

2.1.1 Transmission Dominant Zone

Figure 4 shows the normalized sound pressure distribution plotted against non-dimensional frequency parameter, $k_o a$, for a receiver in the transmission dominant zone:

$$0^o < \beta < \beta_T$$

The curves on figure 4 represent a range of Mach Numbers, from 0.76 to 1.12. Generally, increasing the Mach Number shifts the curve toward lower frequency. As the Mach Number increases, the transmission zone cut-off angle, β_T, is increased. Thus, a receiver at a fixed location is effectively moved closer to the cut-off angle; and, in so doing, sees less of the transmitted noise. The curves in figure 4 are found to collapse to one curve when plotted against:

$$k_o a(\beta_T - \beta)^{-.17}$$

where:

β = observer angle (radians)

$\beta_T = \sin^{-1} \left(\frac{c_o/c_1}{1 + M}\right)$

$= F\ (M^{-1})$

2.1.2 Diffraction Dominant Zone

Figure 5 shows the normalized sound pressure as a function of frequency for a receiver in the diffraction dominant zone,

$$\beta_D < \beta < 90^o$$

Figure 5 shows that the effect of increasing the Mach Number is to shift the curve toward higher frequencies. The curves approach a high frequency assymptotic curve which is independent of Mach Number. The curves in figure 5 are found to collapse to one curve when plotted

against:

$$k_o a(\beta - \beta_D)^{-1.96}$$

where:

$$\beta_D = \sin^{-1}\left(\frac{c_o/c_1}{M}\right)$$

$$= F(M^{-1})$$

2.2 Spacing Ratio

The spacing between the source and the shielding jet is expected to affect the sound pressure in the shadow zone. This effect is investigated in this section.

2.2.1 Transmission Dominant Zone

At $\beta = 0$, the expression for the total sound pressure reduces to the expression derived for the 2-dimensional case of cylindrical wave incident on the jet [10]. It was shown that the effect of decreasing the separation between the source and the jet is to shift the normalized sound pressure curves toward lower frequencies, as shown in figure 6. It was further found that the curves in figure 6 collapse to one curve when the normalized pressure is plotted against the modified frequency parameter:

$$(k_o a) \quad \left(\frac{S}{D}\right)^{-.2}$$

Thus, the effect of increasing the spacing ratio is to shift the sound pressure curve toward higher frequency at a rate proportional to the spacing ratio to the 1/5th power.

2.2.2 Diffraction Dominant Zone

Figure 7 is a plot of the normalized sound pressure at values of $0.667 < S/D < 5.333$ evaluated at $\beta = \beta_D$. The various curves are all relatively constant over the frequency range shown.

The effect of increasing S/D is to shift the curves toward higher

valued of sound pressure. This is consistent with barrier theory where the attenuation in the shadow zone of the barrier decreases as the source moves away from the barrier. From barrier theory considerations, it is expected that the noise reduction in the shadow zone is a function of the included angle subtended by rays projected from the source to the top and bottom edges of the barrier. It is found, based on the data shown in figure 7, that the normalized sound pressure level, ΔSPL, is proportional to the shadow forming angle, where:

$$\Delta SPL = 10 \log \left| \frac{P_T}{P_{in}} \right|^2 = -20\theta_s - 2.76 \text{ (dB)} \qquad (22)$$

where:

$$\theta_s = \sin^{-1}(a/S) \quad \text{(rad)}$$

2.3 Temperature

The diffraction zone cut-off is related to the jet temperature in that the speed of sound in the jet is proportional to $(T_1)^{\frac{1}{2}}$. Thus, as the jet temperature is decreased, the cut-off angle increases. The expected result of increasing the jet temperature is to shift the curve toward higher frequency. This result is shown in figure 8. The plots in figure 8 also show that the curves coalesce to a high frequency assymptote which is temperature independent. The assymptote is, however, dependent on the spacing ratio.

Figure 9 shows the two curves normalized against the parameter:

$$k_o a(\beta - \beta_D)^{-1.96}$$

where:

$$\beta_D = \sin^{-1}\left(\frac{c_o/c_1}{M}\right)$$

$$= F(T_1^{-\frac{1}{2}})$$

The solid line on the figure is the curve showing the expected values for S/D = 2.667.

V. MODIFIED JET SOURCE MODEL

The model as developed in the previous section shows the change in sound pressure at a far field receiver due to a jet of heated flow. In order to estimate the sound level at the receiver, it is necessary to model the noise emission of the actual jet. The modification of the source term in equation 15 is intended to represent the directional nature of the jet noise radiation pattern. The source strength, Q_o, is redefined with a directivity imposed. The modified source term incorporates not only the spatial variation of the jet noise, but also the frequency spectrum.

1. Description of the Jet Noise Model

The source term in the wave equation has the form:

$$\frac{Q_o}{r} e^{-i\omega t} \delta(r-r_o)\delta(\theta)\delta(z)$$

For a point noise source, the source strength, Q_o, is constant. The jet noise model is developed by a formulation for the source strength in which the directivity is imposed. Figure 10 shows a typical plot of polar directivity of the jet noise from measurements by Yu and Dosanjh (11). In the figure, the sound pressure at the polar coordinate is normalized by the sound pressure at the peak.

As shown in figure 10, the far field sound pressure level contours are characterized by a peak, located between 25° and 30° from the jet axis, and diminishing values on either side of the peak. Physically, this states that , due to the convection effect, the sound waves are crowded in the downstream direction and more widely spaced in the upstream direction. This enhances the intensity in directions

making an acute angle with the flow. At the same time, sound rays are refracted by the mean flow, weakening the sound along the core of the jet. Thus, the sound pressure near the jet axis is dominated by this refractive bending of the sound waves.

The general form of the noise source model selected for the present study is suggested by Ribner's analysis (12). The far field mean square sound pressure is made up of a basic directivity function, which defines the spectral shape, and a convection factor. The convection factor is the Lighthill convection factor modified to show the amplification downstream due to the source convection. The source amplitude, Q, based on Ribner's model is:

$$Q = \frac{U_j^4 D}{c_o^2} \, DI(CS, \beta)^{\frac{1}{2}} \, C^{-5/2} \qquad (23)$$

where:

$\frac{U_j^4 D}{c_o^2}$ = amplitude based on Lighthill's U_j^8 velocity dependence

DI = the basic directivity function

CS = modified Strouhal number = CfD/U_j

C = the basic convection factor

$= [(1-M_c \sin\beta)^2 + \alpha^2 M_c^2]^{\frac{1}{2}}$

M_c = effective average source convection speed/c_o

$= 1.5U_j/c_o$

α = non-dimensional parameter

1.1 Basic Directivity Model

Ribner suggests that the basic directivity function is composed of two spectral components. One component is a function of self-noise due to turbulence alone; while the other is a shear noise term arising

from a cross coupling of the turbulence with the mean flow shear. The basic form of the directivity function has been modified by Kim [13] in order to improve the fit to experimental data, where:

$$DI(\beta_n, CS) = \left[A(CS)\ \left(\frac{1+3\cos^2\beta_n}{4}\right) + B(CS)\ (8\cos^3\beta \sin^6\beta_n)\right]^{\frac{1}{2}} \quad (24)$$

where:

A = spectral amplitude due to self-noise

B = spectral amplitude due to shear noise.

1.2 Spectral Amplitude Functions

The choice of A and B for the best fit with the experimental data has been studied by Nosseir and Ribner (14). It is observed that the values of A and B fall on two reasonably smooth curves: the self-noise spectral peak lies roughly an octave above the shear noise spectral peak. This is based on the argument that the spectral component, $e^{2i\omega t}$, in shear noise appears as $e^{i\omega t}$ in the self noise due to squaring of the turbulent velocity component.

Thus,

$$B(CS) = 2A(2CS)$$

Thus the two amplitude functions have the same shape. The shear noise spectrum is shifted by an octave and its amplitude is twice that of the self noise. Ribner (12) assumes that a semi-empirical spectral shape function with the correct assymptotic behavior has the form:

$$\frac{\nu^2}{(1+\nu^2)^2}$$

where:

$$\nu = 2\pi\ CS$$

The specific form of the spectral amplitude functions was obtained by comparison to experimental data of Tanna and Dean (15), shown in Figures 11 and 12, for an isothermal jet ($T_j = T_o$). Variations of 1/3 octave spectral shapes at 30° and 90° from the jet axis where the Mach number is varied from 0.5 to 1.95, is investigated. Tanna and Dean observe that at $\beta = 0^\circ$, the spectral shape has a broad peak. In contrast, at $\beta = 60^\circ$, the spectrum shifts toward lower frequency and the peak becomes more marked.

Kim [15] has found the best fit to experimental data to be made using the amplitude functions:

$$A(\nu) = \frac{(\nu/4)^2}{[1 + (\nu/4)^2]^{1/2}} \tag{25a}$$

$$B(\nu) = \frac{2(\nu/2)^2}{[1 + (\nu/2)^2]^{1/2}} \tag{25b}$$

The estimated spectral shapes are shown by the solid lines on figures 11 and 12. In figure 10 at $\beta = 0^\circ$, the model estimates the trend of the curves to decrease in intensity as flow speed decreases. The agreement between the model and experiment is good at frequencies less than the peak for all flow speeds. The model estimates a greater roll off of sound intensity at high frequency than is measured. At $\beta = 60^\circ$, the polar location at which the overall jet noise is most intense, the estimate shows good agreement with experiment for $U_j/c < 1$. For $U_j/c > 1$, the model is more sensitive to changes in flow speed than experiment indicates. While the estimated spectra are narrower than those estimated at $\beta = 0^\circ$, they are broader than the measured spectra. Finally, the shift toward higher frequency of the peak noise with increasing flow speed is greater in the model than is measured. The estimate peak occurs at a frequency between $1\frac{1}{2}$ and 2

decades higher than is found experimentally at the higher flow speeds.

Since the peak of the overall jet noise pattern is located at a polar location of approximately 30° from the jet axis, the estimated shielding is expected to be most sensitive to the source noise spectrum at $\beta = 60^{\circ}$. From figure 12, the spectral amplitude function is expected to be most reliable for subsonic jet flows for the isothermal jet.

The formulation of the jet noise source strength, Q, incorporates the directivity pattern, convection effect, velocity dependence and spectral shape function. This semi-emperical term is summarized below:

$$Q = \frac{U_j^4 D}{c_o^2}\left[\frac{(\nu/4)^2}{[1+(\nu/4)^2]^2}\frac{(1+3\cos^2\beta_n)}{4} + \frac{16(\nu/2)^2}{[1+(\nu/2)^2]}(\cos^2\beta_n \sin^6\beta_n)\right]^{1/2} \quad (26)$$

$$X\ C^{-5/2}$$

The far field noise radiation estimated using the source term above is compared to experimental data of Yu and Dosanjh [11]. The jet operating conditions are:

$M_j = 1.5$

$T_j = 365.8^{\circ}R$

$T_o = 530.4^{\circ}R$

Figures 13, 14 and 15 show the polar directivity of the jet noise. In the figure, the sound pressure is normalized by the sound pressure at the peak location. The data in figure 13 are measured at a Strouhal number, St = 0.12, where:

$$St = \frac{fD}{U_j}$$

in which:

f = frequency

D = jet diameter

U_j = jet exit velocity

Figure 14 is measured at St = 0.25 and figure 15 is for St = 0.5.

The figures generally show good agreement with the measured jet noise pattern. The model estimates the location of the peak and the rapid decrease in sound pressure level on either side of the peak. The rate of sound reduction on either side of the peak follows the measured data.

The model for the source strength representative of a jet has been developed. The model consists of a convection factor, which shows the downstream amplification due to source convection; a basic directivity function which defines the spectral shape; and an amplitude based on Lighthill's U_j^8 velocity dependence. The model estimates the polar directivity of a cold, supersonic jet for a range of frequencies corresponding to Strouhal numbers from 0.12 to 0.5. The model estimates the form of the spectral amplitude and the relative amplitude dependence on velocity of an isothermal jet at subsonic flow. The model for the spectral amplitude is found to deviate from measured data at supersonic flows for the isothermal jet, at a location near the jet noise peak. This is not felt to be due to an error in the form of the spectral function; but rather to the choice of parameters. It is felt that the relationship, $\nu/4$, in the basic amplitude function makes the function over-sensitive to changes in flow speed. A relationship closer to $\nu/2$. as suggested by Ribner, makes the function less sensitive to flow speed change; which is the

trend of the experimental data.

The form of the source strength is preferred because of its adaptability to the shielding model originally developed. No change in the basic formation of the model is necessitated. The estimated sound pressure at the receiver is still based on a point noise source. However, with the modified source model, the source strength is a function, not only of the characteristics of the jet, but also of the receiver location.

2. Comparison to Heated Jet Spectra

Figure 16 and 17 are spectral distributions downstream of a heated jet. Figure 16 is in the near downstream region, $\beta = 30^{\circ}$; and figure 12 is in the far downstream region, $\beta = 60^{\circ}$. It is assumed that the pattern the same at any radial location around the jet axis. The spectral shapes are compared to data measured by Kantola [16] for the following jet operating parameters:

T_o = ambient temperature = $530^{\circ}R$

T_j = jet temperature = $1238^{\circ}R$

U_j = jet exit velocity = 1552 ft/sec

The measured data follow the same trends as were noted for the isothermal jet. In the near downstream region, figure 16, the spectrum is relatively broad. The spectrum peaks becomes more defined further downstream, figure 17, and the peak shifts toward lower frequency. The peak overall sound level is expected to be greatest at approximately 30° from the jet axis. This is reflected in the fact that the maximum sound level at $\beta = 60^{\circ}$ (Figure 17) is 8 dB greater than that measured at $\beta = 30^{\circ}$ (figure 16).

The model estimates a broader spectrum than is measured in the near downstream, figure 16. The spectral peak is also estimated to occur at a frequency higher than is found experimentally.

The model shows better agreement near the location of the peak sound energy, figure 17. The measured and estimated peaks occur at approximately the same frequency, and the spectral shapes are similar. While the model overestimates the maximum sound level for both the near and far downstream locations by approximately 1½ dB, the relative difference in magnitude between the two locations is shown.

VI. MODIFIED SHIELDING JET MODEL

Measurements of the sound pressure level from a source near a jet have been made by Yu and Fratello at NASA-Langley Research Center [17]. Comparison of the measured shielding to the shielding estimated by the model is made in order to test the analytical model. The shielding jet is an isothermal Mach number 0.53 air jet. In the experiments, the noise source is located at a lateral spacing of 2.5 jet diameters from the centerline of the jet and 4 jet diameters downstream from the jet nozzle. The receiver is in the acoustic far field at R 100 jet diameters.

For the purposes of comparison the normalized sound pressure level at a receiver in the acoustic far field is expressed as a directivity function, ΔSPL,

$$\Delta SPL = 10 \log_{10} \left| \frac{P_T}{P_{in}} \right|^2 \quad dB$$

A value of ΔSPL < 0 indicates sound reduction. ΔSPL > 0 indicates amplification.

Figures 18 and 19 show the modification of the directivity function by the shielding jet in azimuthal planes downstream of the source. The curves in figure 18 are for the normalized frequency parameter, $k_o a = 0.56$, and in figure 19, $k_o a = 1.6$.

The model agrees quite well with the experimental data within the transmission zone directly below the source. However, as the receiver moves downstream from the source into the diffraction dominated zone, the model begins to diverge from the experimental data, showing less shielding than experimentally indicated. The model estimates more

diffraction of sound around the jet than is found experimentally. Thus, the experimental jet is a more effective noise barrier far downstream of the jet nozzle as it mixes with the quiescent air surrounding the jet. It is expected that modification of the shielding jet model to include this increased barrier effect will resolve, in large part, the differences in the far downstream region.

1. Development of the Model

The shielding jet model development consists of two parts: spreading parameter and velocity approximation. In the shielding analysis, at any downstream location, the jet is modelled as an infinite cylinder, as was done in the original derivation. However, the diameter of the cylinder is matched to that of the real diverging jet at the station where the line of sight from the source to the receiver cuts the middle of the mixing region of the real jet. Associated with the jet widening is a decay of the centerline velocity and a distrotion of the flow profile across the jet cross-section. A slug flow velocity is obtained by matching the volumetric flow rate through the jet cross-section to the equivalent uniform velocity through the cross-section at that station.

The free turbulent jet most often encountered is one with a uniform velocity profile in the initial cross-section of the jet, spreading into a medium at rest. Such a jet is shown in figure 20. The boundaries of the jet form diverging surfaces which intersect at the edge of the nozzle. These boundaries are composed of a complex turbulent mixing layer that is multifunctionally jet dependent, making the boundaries of the jet difficult to predict. Various independent, empircal formulations describing the jet have been correlated in an

attempt to arrive at a simple functionally dependent representation of the jet flow.

The initial region of the jet is termed the potential core and extends approximately 5 diameters downstream. Due to the fundamental property of constant static pressure throughout the jet in this region, the potential core has the unique characteristic of constant velocity equal to the velocity at the jet exit [18]. Downstream of the jet exit, the boundaries thicken due to entrainment of particles from the surrounding medium, and the slowing of the particles within the jet flow. This leads to an increase in the cross-section of the jet, and a gradual deterioration of the nonviscous core of potential flow.

The zone immediately following the potential core is the transition region extending to 8 diameters downstream. In this region, the axial velocity begins to decay as the transverse velocity profile assumes a flatter, wider more nearly Gaussian shape. The transition region extends to the fully developed region, at which point the velocity profiles become similar in shape.

1.1 Spreading Parameter

Several different values have been experimentally determined for the spread rate of an isothermal jet. An often cited spread rate is a constant value agreed upon by Spencer and Jones (19), Liepman and Laufer (20), and Brown and Roshko (21) of approximately .165. This corresponds to an included angle for the jet spread of 18 degrees.

This general linear spread rate of the mixing layer can be modified as a function of Mach number. The Mach number dependent jet

radius relationship suggested by Lau, Morris, and Fisher (22):

$$r_b = a + \delta' (x-x_o) \tag{27}$$

where:

δ' = $0.165-0.045\ M_1^2$

M_1 = Mach number

a = Radius of jet nozzle

x_o = virtual origin, chosen to be zero in this analysis

This relationship shows that increasing Mach number decreases the jet spread. From a shielding standpoint, increasing Mach number decreases the effective barrier dimension.

1.2 Velocity Representation

Representation of the velocity in the jet involves two major areas: the centerline velocity decay and the velocity profile across the jet cross-section. From this latter profile the slug flow velocity equivalent is approximated.

1.2.1 Centerline Velocity Approximation

The centerline velocity is estimated respectively for the different regions of the jet, so that a more realistic description of the actual shielding jet is obtained. Within the potential core of the jet, the velocity remains constant and equal to the jet exit velocity. This property is employed in the initial region of the jet to represent the centerline velocity as a constant value:

$$U_m (x) = U_j \qquad (o<x<x_c) \tag{28a}$$

Beyond the potential core, the axial centerline velocity gradually begins to decay. Initially, two alternate correlations were considered to represent the centerline velocity for the transition

region and the fully developed region. Although these relations simulated the actual jet very well within the specified regions, they did not allow for a continuous transition from the transition region to the fully developed region. Hence, an empirical relation by Goerther [23] for the axially decaying centerline velocity is subsequently chosen for the entire downstream region beyond the potential core:

$$U_m(x) = U_j \frac{\sigma}{3.22}\left(\frac{D}{x}\right) \qquad (x>x_c) \tag{28b}$$

where:

$\sigma = 15.2$

When the centerline velocity is evaluated from this equation at the end of the potential core, $x = x_c$, $U_m(x)$ is found to be equal to .964 U_j. This allows for a reasonably smooth transition from the initial region of the jet where $U_m(x)$ is constant, to the transition region of the jet where $U_m(x)$ begins to axially decay. In addition, there is no sudden discontinuity in the centerline velocity between the transition region and the fully developed region.

1.2.2 Velocity Profiles

Different velocity profiles are applied to the different regions of the jet and compared to the experimental trends. The final profile chosen for each specific region is that profile which allows for a continual transition of U_{slug} from region to region.

For the initial region of the jet, $x<x_c$, two different velocity profiles are used. The velocity profile for the region outside of the potential core, is an exponential relation by Schubert [24]:

$$U(r,x) = U_m(x) * \exp\left\{-52.65\ [(r/D - .5)\ D/x + .0946]\right\} \qquad (29a)$$

for:

$$r_1 < r < r_b$$

The velocity profile within the potential core is uniform and is equal to the velocity at the jet exit:

$$U(r,x) = U_1 \qquad (29b)$$

for:

$$r < r_1$$

The velocity profile employed within the transition region of the jet represents the experimental trends [24]:

$$U(x) = U_m(x) * \exp\left\{-2.304\ [r/D/\ (.5 + .1145\ x/D]^2\right\} \qquad (29c)$$

Finally, the velocity profile suggested by Goerther [25] for the fully developed region is:

$$U(x) = U_m(x) * \left\{[1.0 + .25\ (\ r/x)^2\ ]^2\right\}^{-1} \qquad (29d)$$

where:

$$\sigma = 15.2$$

1.2.3 Slug Flow Approximation

The total volumetric flowrate is evaluated by integrating the velocity over the jet cross-section. A slug flow velocity approximation is then determined by dividing the volumetric flowrate by the cross-sectional area of the jet:

$$U_{slug}(x) = 2\pi \int_0^{r_b} U(r,x)\ r\,dr/A(x) \qquad (30)$$

Figure 21 shows both the centerline velocity and the slug flow approximation velocity downstream of jet exit. The centerline velocity shows a discontinuity at the interface between the potential core and the transition region. The slug flow approximation, based on the flow rate is smoother throughout the entire downstream flow

region.

2. Comparison to Experiment

The model with the modified shielding jet is compared to the isothemal air jet shown in a previous section of the paper in order to assess the improvement of the shielding estimate. In addition, comparison is made to experimental results for a higher Mach Number isothermal air jet, and a simulated hot jet using helium as the flow medium. These latter experimental data were provided by Dr. J. C. Yu of NASA Langley Research Center [26].

2.1. Isothermal Jet, M = 0.531

The estimated and experimental azimuthal directivities for the Mach number 0.531 air jet are shown in figure 22 and 23. It is seen that inclusion of the modified shielding jet model has little effect on the estimated attenuation in the near downstream region. This is to be expected because transmission is the dominant shielding mechanism in the near downstream. The effect of jet widening is seen in the far downstream, where diffraction dominates. The model generally shows improved agreement with experiment, particularly on the shadow side of the shielding jet ($\theta = 180$). The model overestimates the shielding at locations approaching the jet axis and at higher frequency (figure 23). This error is approximately 7 dB on the shadow side of the jet. The model generally underestimates the scattering of incident sound toward the bright side of the jet ($\theta = 0^{\circ}$ This error is on the order of 2 dB. Despite these errors, the model with modified shielding jet in general more closely approximates the measured shielding.

2.2 Isothermal Jet, M = 0.886

Increasing flow speed decreases the jet spread rate. This reduces the barrier dimension downstream. However, the increased flow speed increases the effectiveness of the barrier. The former effect decreases shielding and the latter increases it. Thus, it is difficult to predict the expected result of increasing flow speed on shielding. Figures 24, 25 and 26 show the azimuthal directivity for the isothermal air jet at Mach number 0.866. At lower frequency, figure 24, increasing flow speed generally increases shielding on the shadow side of the jet. This trend is also shown by the model. The effect decreases as frequency increases. At $k_o a = 1.6$, the measured shielding is nearly the same as for the M = 0.531 jet (figure 23). The model shows a more consistent trend of increasing shielding for increasing flow speed for all frequencies. From figures 24, 25 and 26 it is seen that the model shows trends similar to experiment, with the curves shifting toward the bright side of the jet as the receiver moves downstream; and with the attenuation increasing with increasing frequency. With the exception of $\beta = 60^\circ$ at $k_o a = 1.6$ (figure 26) the model is within 5 dB of the measured data.

2.3 Simulated Hot Jet

The purpose of the project is to estimate hot jet shielding for aircraft noise propagation. For this reason, the model is compared to a simulated hot jet using helium as the flow medium. For the helium jet, $\rho_1/\rho_o =$ and $c_1/c_o = 3.0$. This corresponds to a jet of heated air of temperature between 2050°K and 2650°K. While this may be considered an extreme case, it is intended to demonstrate the sensitivity of the jet shielding model to temperature variations in

the jet.

The contours plotted show the polar directivity on the shadow side of the shielding jet ($\theta = 180^{\circ}$). The SPL is evaluated for a ranges of angles $-30^{\circ} < \beta < 90^{\circ}$. Thus the shielding is evaluated at both upstream and downstream receiver locations.

The polar directivity is evaluated for the simulated hot jet for $U_1/c_1 = 0.177$ and shown in figure 27. Both the model and experiment indicate shielding upstream of the jet exit, $\beta < 0^{\circ}$. The agreement between model and experiment is favorable at upstream locations. The model shows relatively uniform shielding for downstream locations until $\beta = 16.5^{\circ}$, when the shielding increases rapidly. This angle corresponds to the transmission zone cut-off angle, eqn. 15. At low frequency, the drop off in Sound Pressure Level is rapid but reaches an inflection point at $\beta = 30^{\circ}$, and begins to rise at further downstream locations. This indicates that the sound is diffracting around the jet. The normalized Sound Pressure Level would approach an assymptotic value far downstream, except that continued jet widening blocks this diffraction. The experimental data show the same trend with the rate of decrease of Sound Level increasing at locations downstream of approximately 16.5°. The inflection occurs at the same location as the model, but the trough is not as deep, and the attenuation is not as much in the far downstream.

At higher frequency $k_o a = 1.6$, the roll-off beyond the transmission zone cut-off angle is more gradual and shows a smoother trend indicating that diffraction around the jet is a less dominant factor. This is to be expected from barrier theory, where diffraction

around the barrier is felt more strongly at lower frequencies. The agreement between experiment and the model is quite good for downstream angles up to $\beta = 45^{\circ}$. As with the lower frequency case, the model overestimates the shielding deep in the downstream region. If was observed [26] during the jet shielding experiment that at angles closer to the jet axis than 45° the measured Sound Pressure Level exhibited wide fluctuations. This is due to the strong turbulence at the interface between the jet and the quiescent air due to mixing of the two media. In addition to causing scatter in the measured data, the turbulence is expected to reduce the effective width of the jet and thus its efficiency as a noise barrier. It may thus be expected that a jet in which the temperature difference is not as great may exhibit shielding behavior more similar to that estimated.

VII. ESTIMATE OF TWIN-JET SHIELDING

The model is compared to measured jet-by-jet shielding [16]. The experimental data were collected by Kantola for twin round jets with the following operating conditions:

V_1 = 1552 ft/sec

T_1 = 1238 ^{o}R

T_o = 530 ^{o}R

S/D = 2.667

The ΔSPL is evaluated by comparing the Sound Pressure Level at $\theta = 180^{o}$, to the Sound Pressure Level from a single source plans 3 dB. This latter sound level is equivalent to the noise emission from two equal sources with no interaction.

In the case of shielding of a point noise source which was considered in previous sections, the noise emitted by the shielding jet was not affected by the source. In twin jet configuration, the source is a jet which reflects sound energy emitted by the shielding jet. This interaction between the source and shielding jets is shown in figure 28. The total sound pressure at the far field receiver includes the ray from the shielding jet, P_1, and the ray from the source jet, P_2, which is scattered by the shielding jet. In addition, a ray emitted from the shielding jet is reflected by the source jet and thus reflected ray is then scattered as it passes by the shielding jet, P_3. Other rays arrive at the receiver after multiple reflections between the two jets. As a first approximation, only this first reflected ray will be considered in the simulation of the jet-by-jet shielding. The strength of the virtual source which emits ray P_3 is

evaluated by calculating the energy of the ray emitted into free space after reflection from the jet. That is, the strength is the magnitude of the total sound pressure from a point noise source impinging on a single jet, where the receiver is in the bright zone of the jet.

The measured and estimated values are shown in figure 29, where the jet-by-jet shielding is evaluated at 30° from the jet axis ($\beta = 60^{\circ}$) and 60° from the jet axis ($\beta = 30^{\circ}$). The jet widening algorithm is included in the estimated ΔSPL. In the near downstream region, $\beta = 30^{\circ}$, the model estimates that the shielding jet has little influence at low frequency. Thus, the sound from the source jet and the sound from the shielding jet which is reflected by the source jet are both of approximately equal magnitude and the combined rays do not "see" the shielding jet because the wave-length is much greater than the jet diameter at a normalized frequency of approximately 0.3, the sound level drops off sharply. This behavior is characteristic of the normalized sound pressure in the transmission dominant zone. The measured ΔSPL does not show the sharp break at $k_o a = 0.3$. The curve is generally smoother in frequency.

The observed differences in trend suggest that higher order reflections of sound rays between the two jets may be more significant, particularly at higher frequencies, corresponding to $k_o a > 0.6$.

When the receiver is closer to the jet axis, $\beta = 60^{\circ}$, the decrease in normalized sound level is more gradual in frequency, as is expected for the diffraction dominant zone. The high frequency oscillation shown is more characteristic of the transmission phenomenon. This oscillation is not felt to be due to an instalibity

in the model. The analytical model shows better agreement with the experiment in the far downstream regions, falling generally withing ±2 dB of the measured values for frequencies corresponding the $k_o a < 2.0$. At frequencies above $k_o a = 2.0$, the peaks of the oscillating sound pressure level agree with measured values. If the valleys were mashed by other noise sources during the data collection, the absence of these oscillations in the higher frequencies is explained.

REFERENCES

1. Ribner, H.S., "Reflection, Transmission, and Amplifcation of sound by a Moving Medium", JASA vol. 29, no. 4, p. 435.

2. Miles, J.W., "On the Refliction of Sound at an Interface of Relative Motion", JASA vol. 29, no. 2, p. 226.

3. Yeh, C., "Reflection and Transmission of Sound Waved by a Moving Fluid Layer", JASA vol. 41, no. 4, p. 817.

4. Yeh, C., "A further Note on the Reflection and Transmission of Sound Waves by a Moving Fluid Layer", JASA vol. 43, no. 6, p. 1454.

5. Parthasarathy, S.P., Cuffel, R.F., and massier, P.F., "Twin Jet Study, Final Report", Jet Propulsion Laboratory: California Institute of Technology, Pasadena, California, November 3, 1978.

6. Candel, S. and Julienne, A., "Shielding and Scattering by a Jet Flow", 3rd AIAA Aero-Acoustics Conference, Palo Alto, California. July, 20-23, 1976.

7. Jefferies, H. and Jefferies, B., "Methods of Mathematical Physics", Cambridge University Press, 1956.

8. Kinsler, L.E., and Frey, A.R., "Fundamentals of Acoustics", Second Ed. John Wiley and Sons Co., 1962.

9. Bowman, J.J., Senior T.B.A., and Uslenghi, P.L.E., eds., "Electromagnetic and Acoustic Scattering by Simple Shape", North-Holland Publishing Co., Amsterdam. 1969.

10. Gerhold, C.H., "Two-Dimensionaal Analytical Model of Twin Jet Shielding", JASA vol. 69, no. 4, pp. 904-908, (1981).

11. Yu, J.C. and Dosanjh, D.S., "Noise Field of Coaxial Interfacing Supersonic Jet Flaws", AIAA paper no. 71-152, 1971.

12. Ribner, H.S. "The Generation of Sound by Turbulent Jets. Advances", Applied Mechanics, vol. VIII, pp. 103-182, 1964, Academic Press, New York, N.Y.

13. Kim, Changho, "Three-Dimensional Study of Twin-Jet Shielding", M.S. Thesis, Texas A&M University, May 1982.

14. Nosseir, N.S.M., Ribner, H.S., "Tests of a Theoretical Model of Subsonic Jet Noise", AIAA paper pp. 75-436, Mar., 1975.

15. Tanna, H.K., Dean, P.D., "An Experimental Study of Shock-Free Supersonic Jet Noise", AIAA paper 75-480, Mar., 1975.

16. Kantola, R.A., "Shielding Aspects of Heated Twin Jet Noise", AIAA

4th Aeroacoustics Conference. Atlanta, GA., Oct. 3-5, 1977.

17. Yu, J.C. and Fratello, D.J., "Measurement of Acoustic Shielding by a Turbulent Jet", AIAA paper number 81-2019, 1981.

18. Abramovich, G.N., "The Theory of Turbulent Jets", MIT Press, 1963.

19. Spencer, B.W., and Jones, B.G., "Statistical Investigation of Pressure and Velocity Fields in Turbulent Two-Stream Mixing Layer", AIAA paper no. 71-613, 1971.

20. Liepman, H.W., and Laufer, J., "Investigation of Free Turbulent Mixing", NACA Technical note 1257, 1947.

21. Brown, G.L., and Roshko, A., "On Density Effects and Large Structure in Turbulent Mixing Layer", Journal of Fluid Mech., vol. 19, pp. 591-624, 1974.

22. Lau, J.C., Morris, P.J., and Fisher, M.J., "Measurements in Subsonic and Supersonic Free Jets Using a Laser Velocimeter", Journal of Fluid Mech., vol. 93, pp. 1-27, 1979.

23. Rajaratnam, N., "Turbulent Jets", Elsevier Scientific Publishing Co., 1976, p. 44.

24. Schubert, L.K., "Numerical Study of Sound Refraction by a Jet Flow - I. Ray Acostics", Journal of Acoustic Society of America, vol. 51, no. 2, (part 1), pp. 439-446.

25. White, F.M., "Viscous Fluid Flow", McGraw-Hill, 1974, p. 510.

26. Yu, J.C., Private Correspondence.

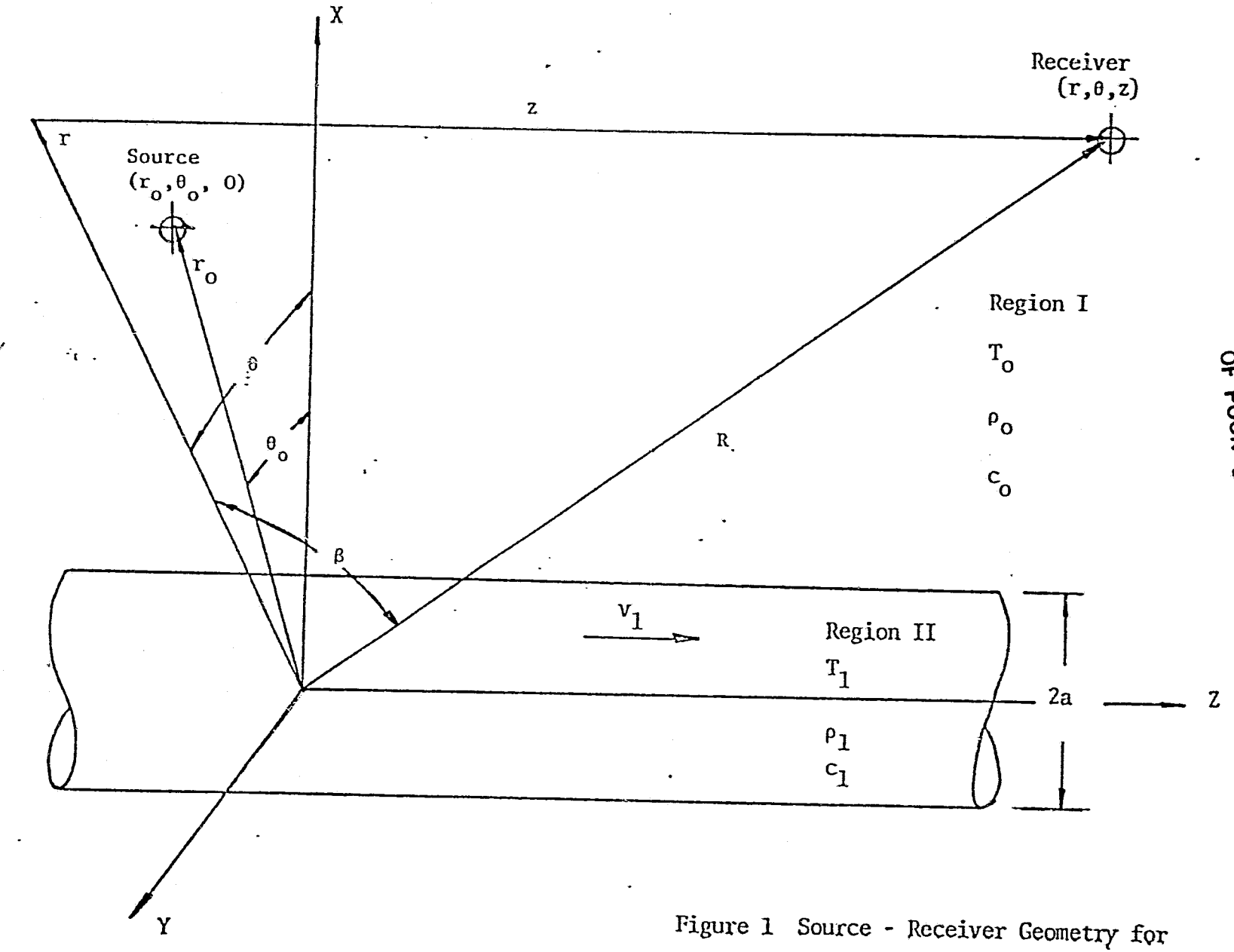

Figure 1 Source - Receiver Geometry for Jet Shielding Analysis.

ORIGINAL PAGE IS OF POOR QUALITY

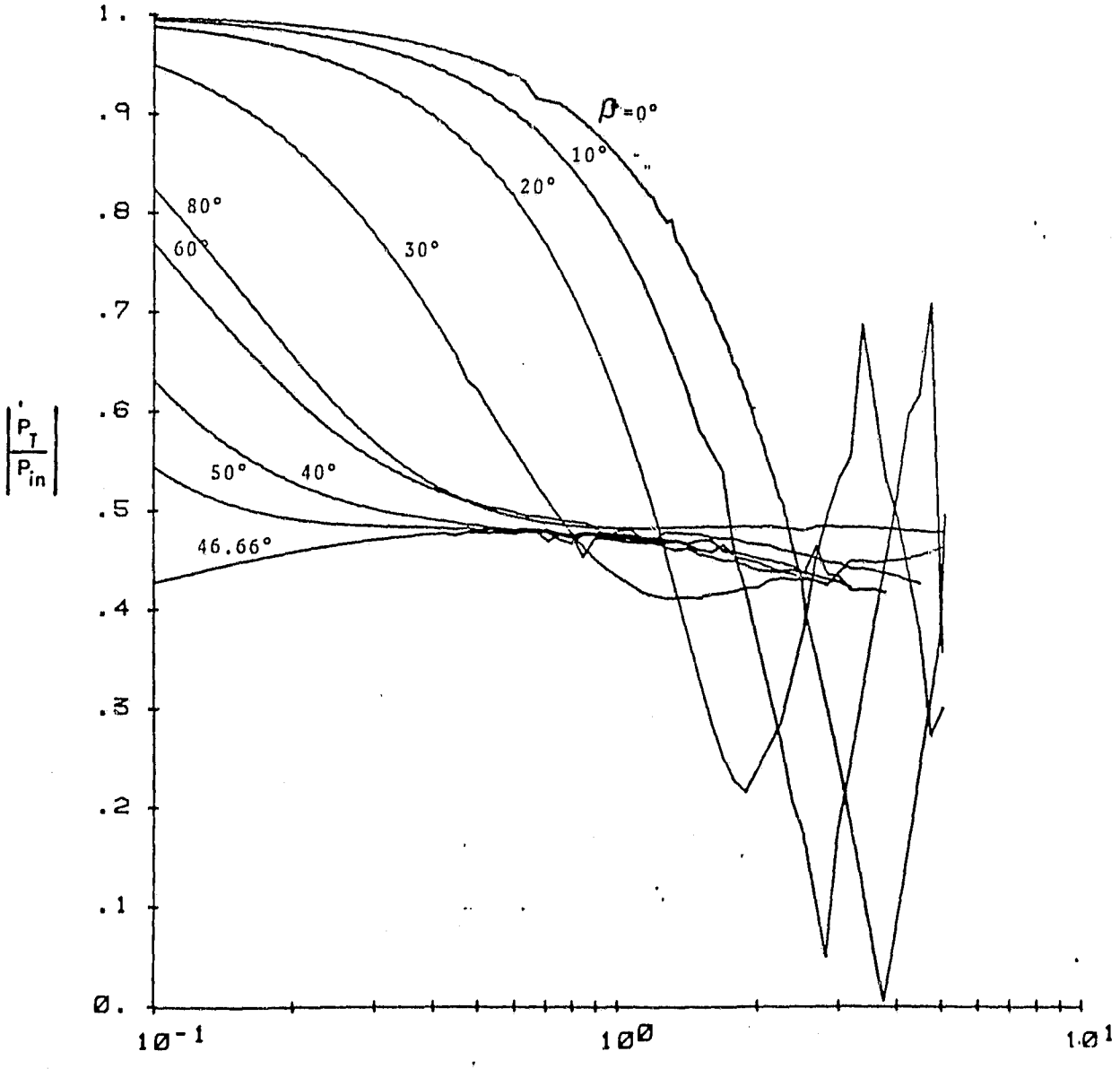

Figure 2. Normalized Sound Pressure in Shadow Zone of Hot Jet.

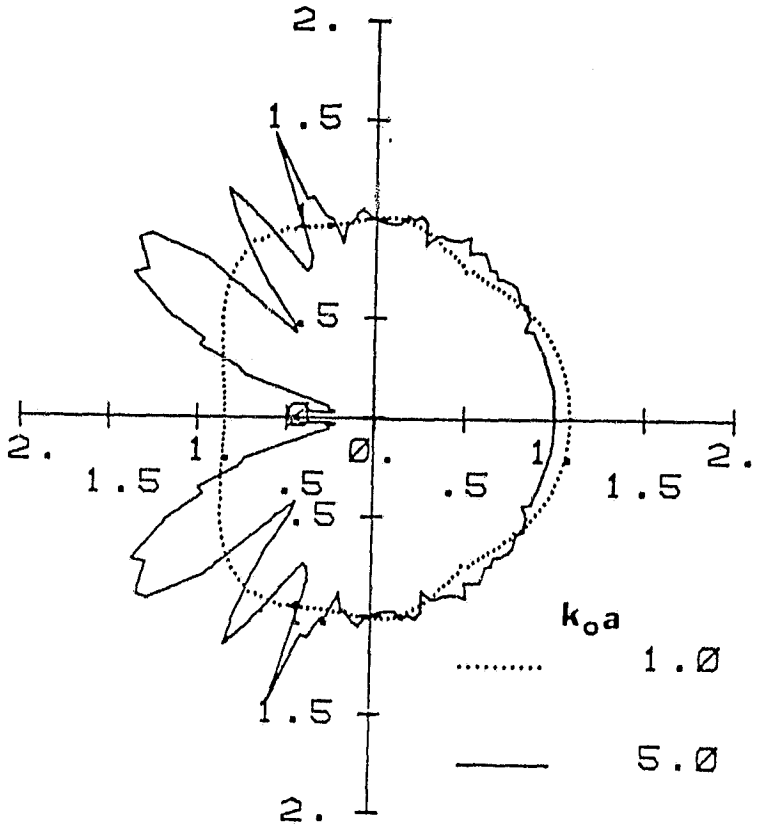

Figure 3. Azimuthal Variation of Normalized Sound Pressure in near downstream (Transmission Dominant) region. Shielding jet is at the intersection of the axes.

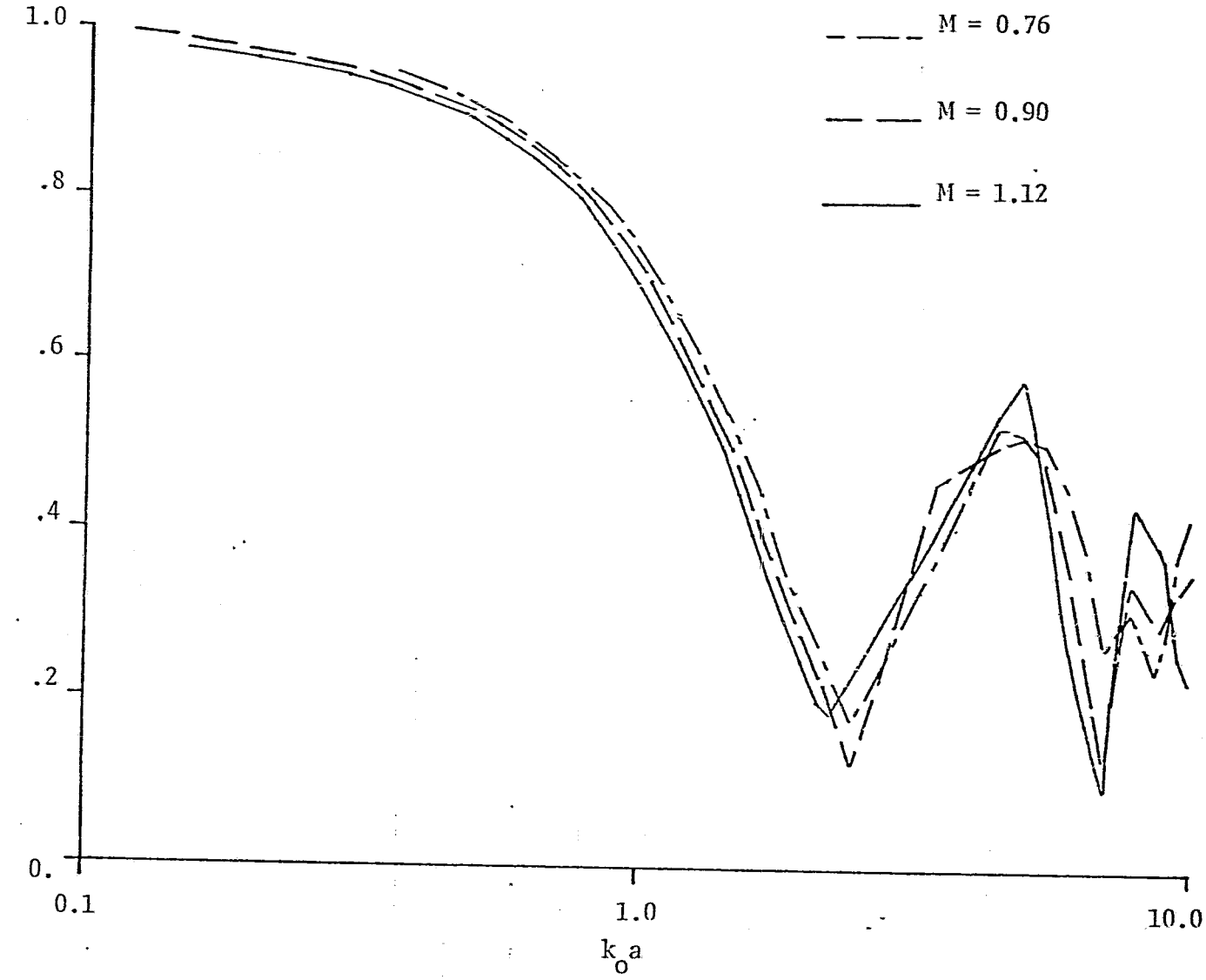

Figure 4. Variation of Normalized Sound Pressure with Non dimensional Frequency Receiver in Transmission Dominant Zone. Spacing Ratio, S/D = 2.667

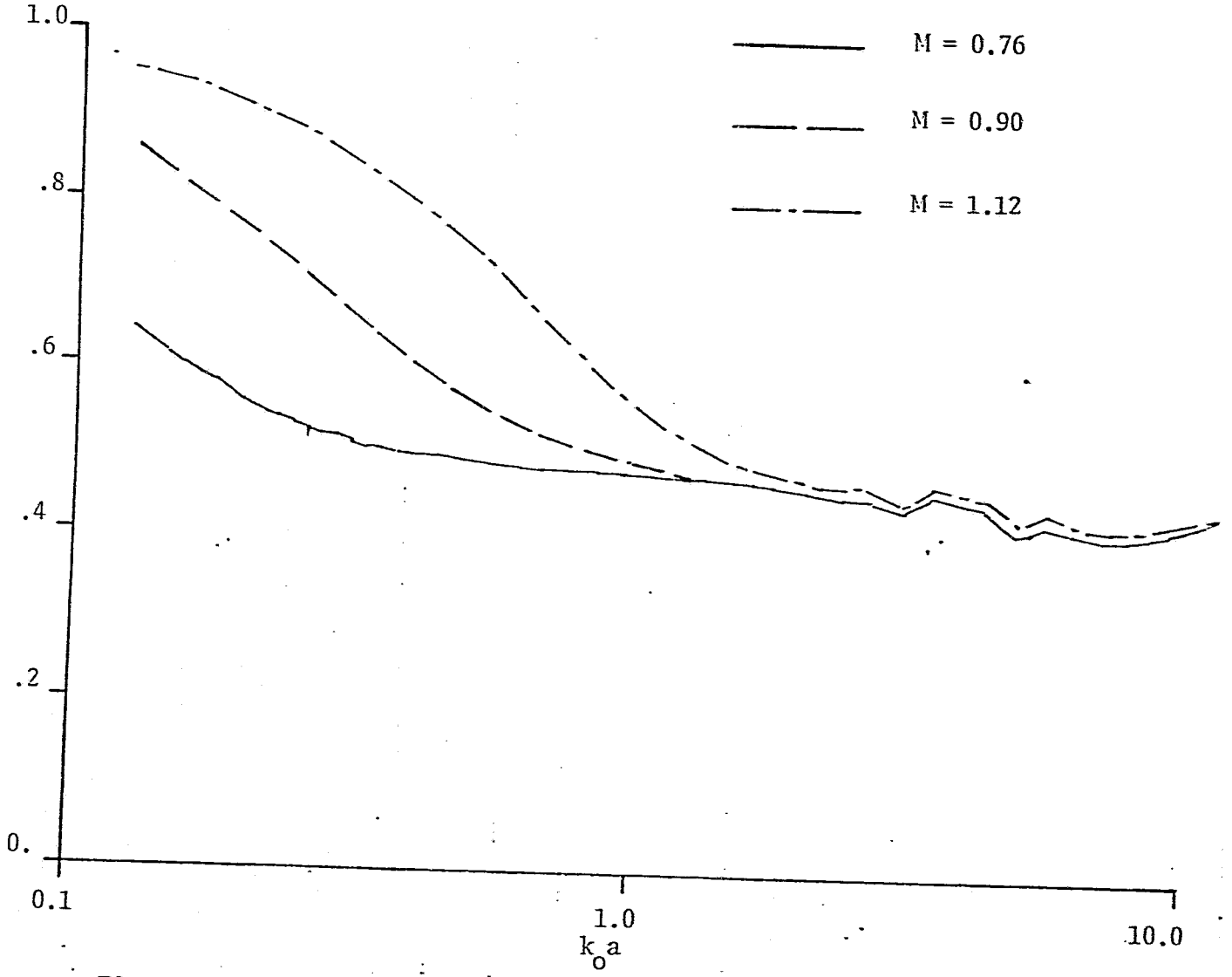

Figure 5. Variation of Normalized Sound Pressure with Non-dimensional Frequency. Receiver in Diffraction Dominant Zone. Spacing Ratio, $\frac{S}{D} = 2.667$

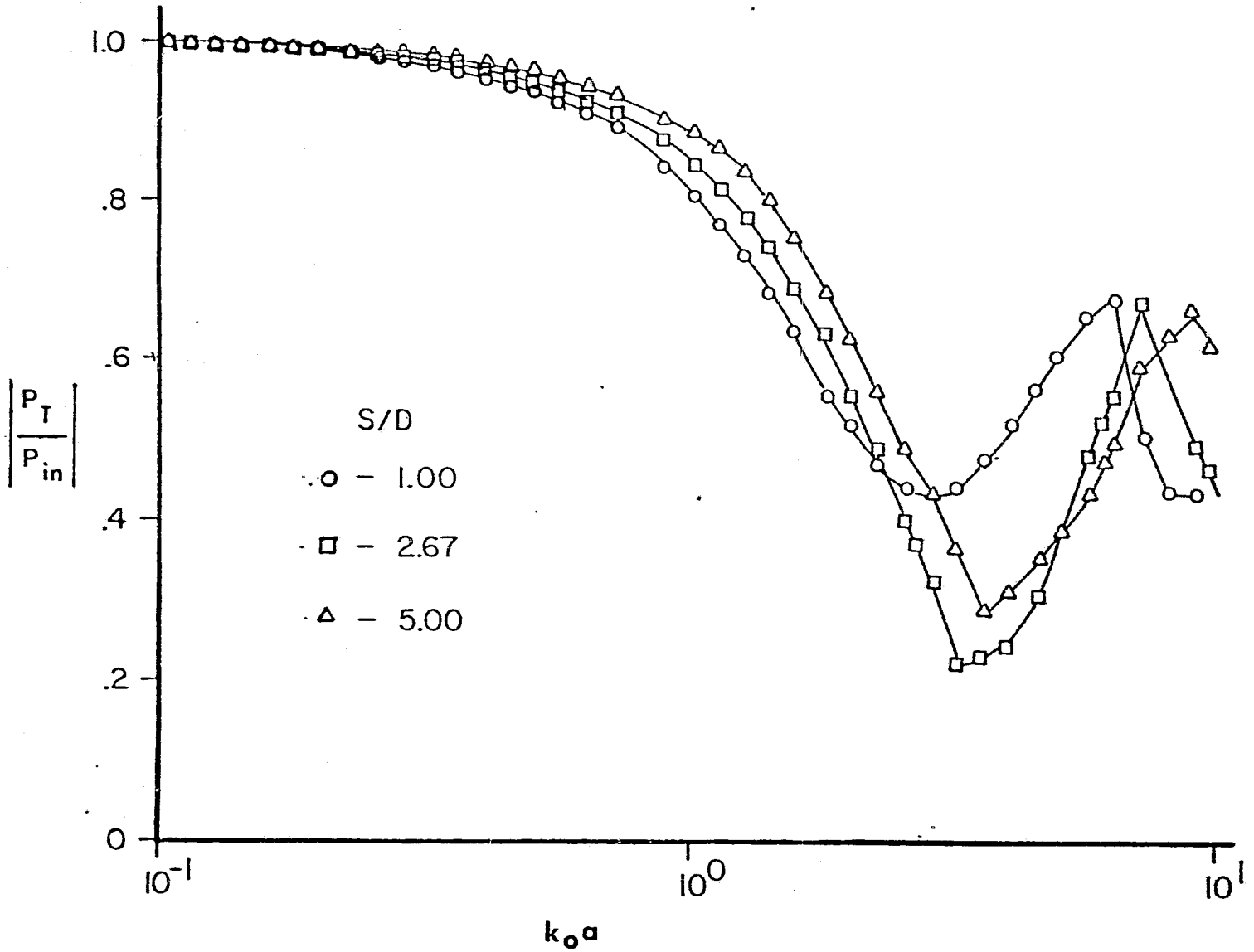

Figure 6. Variation of normalized sound pressure with spacing ration; two-dimensional model.

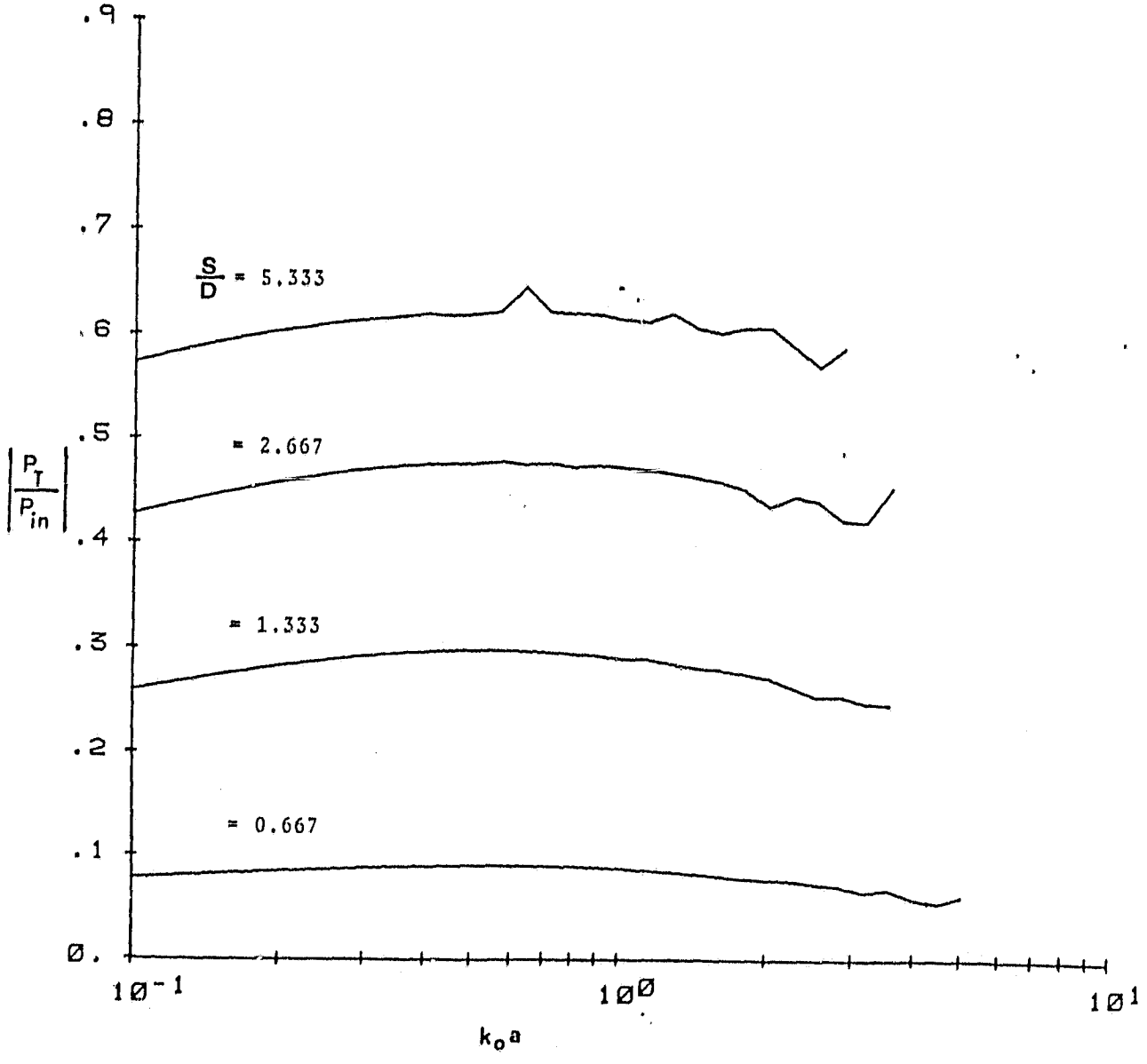

Figure 7. Normalized sound pressure in shadow zone at diffraction cut-off angle; effect of spacing ratio.

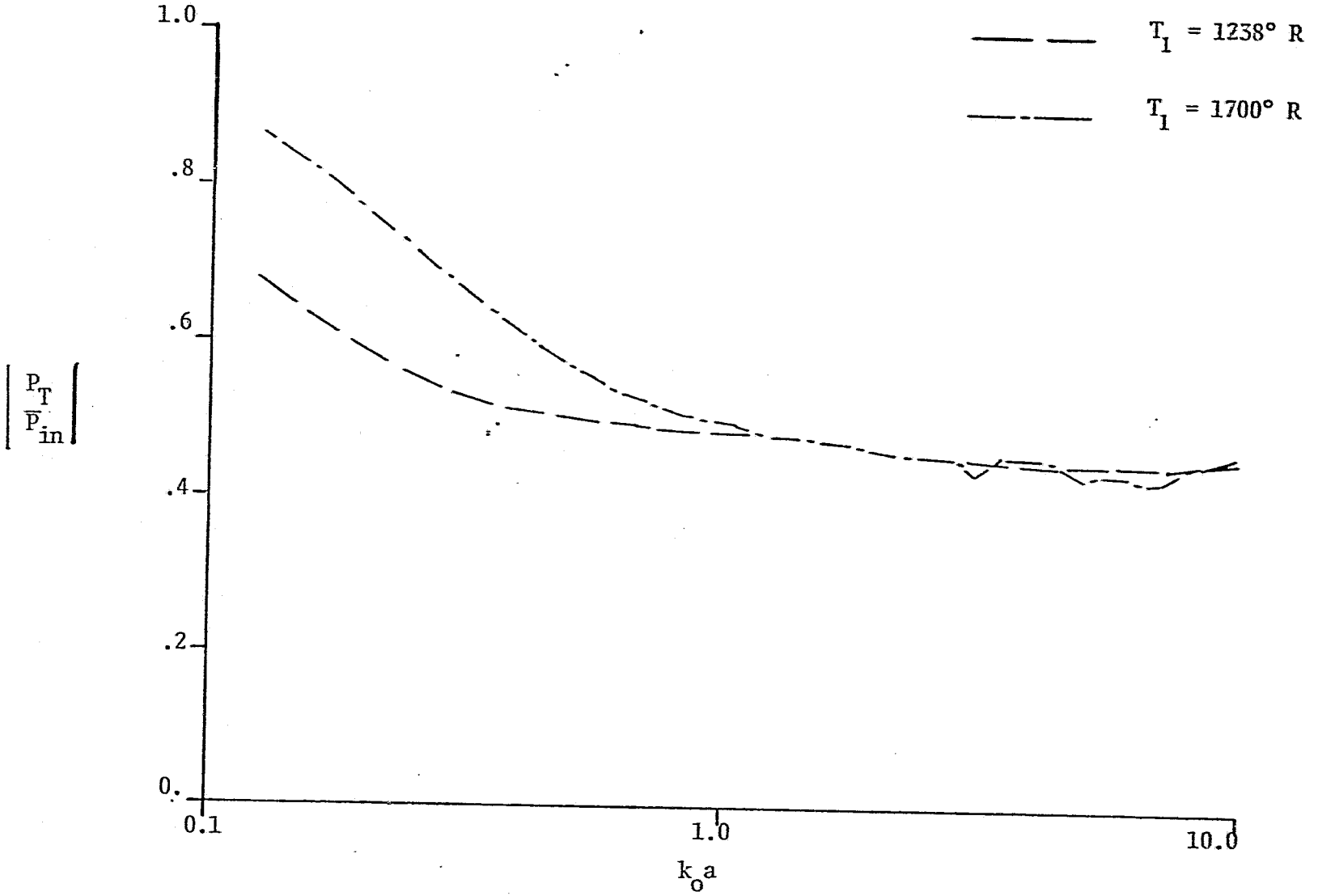

Figure 8. Variation of Normalized Sound Pressure with Non-dimensional Frequency . Receiver in Diffraction Dominant Zone. Spacing Ratio, $\frac{S}{D}$ = 2.667.

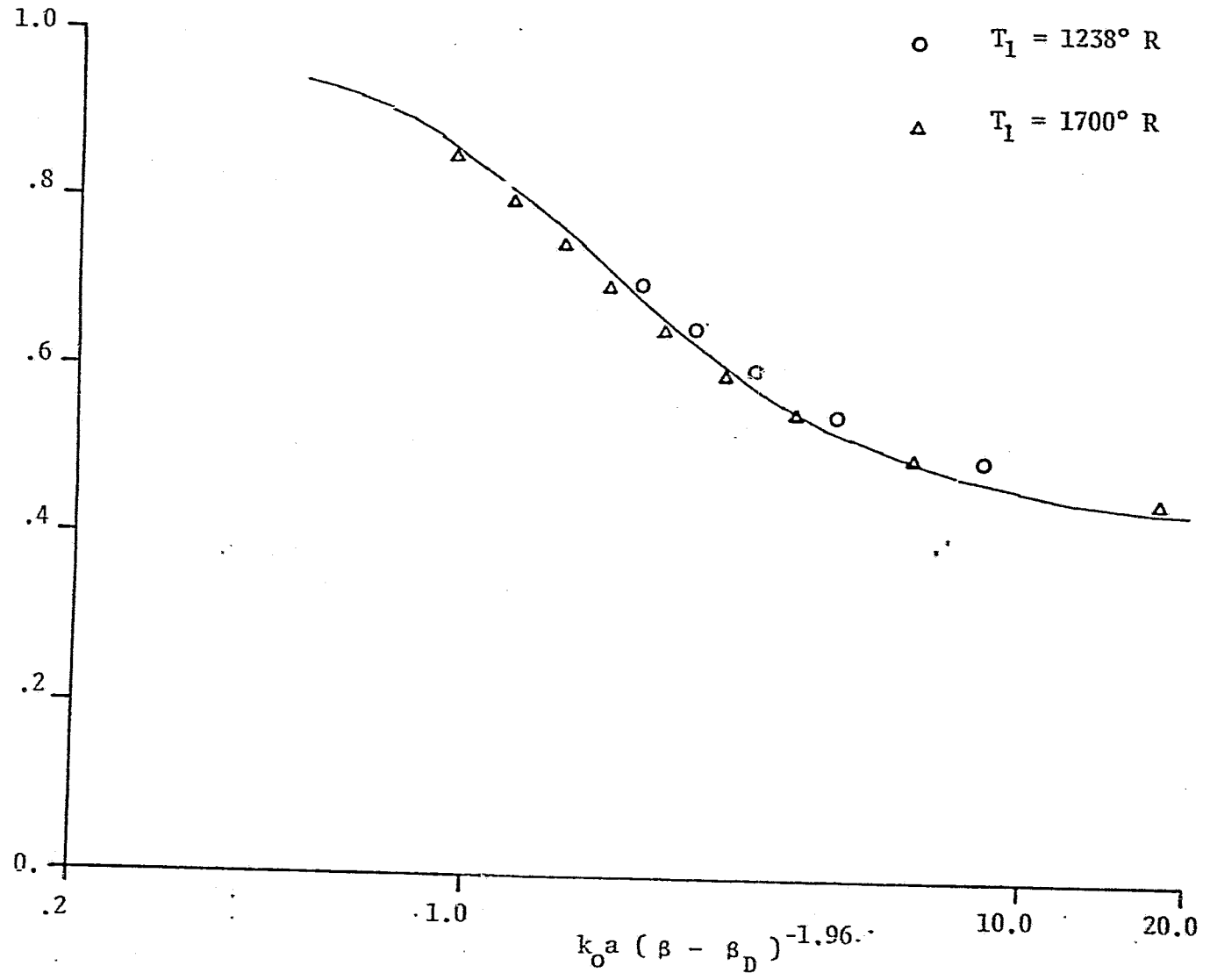

Figure 9. Plot Showing Normalization of Jet Temperature Effect. Solid Line is Normalized Sound Pressure Contour for S/D = 2.667, from Figure 9.

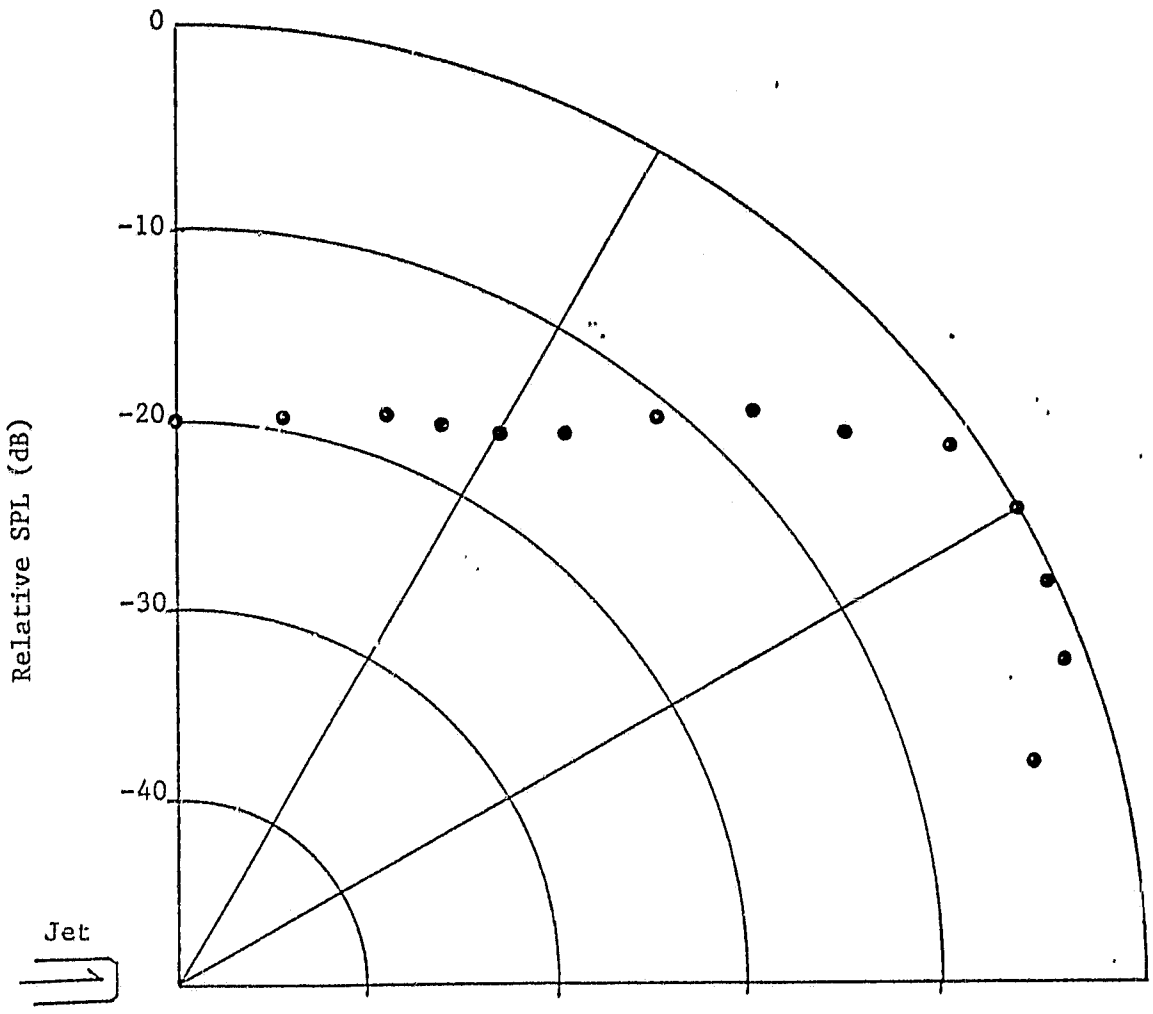

Figure 10. Typical Polar Directivity Plot of Unheated, Supersonic Jet.

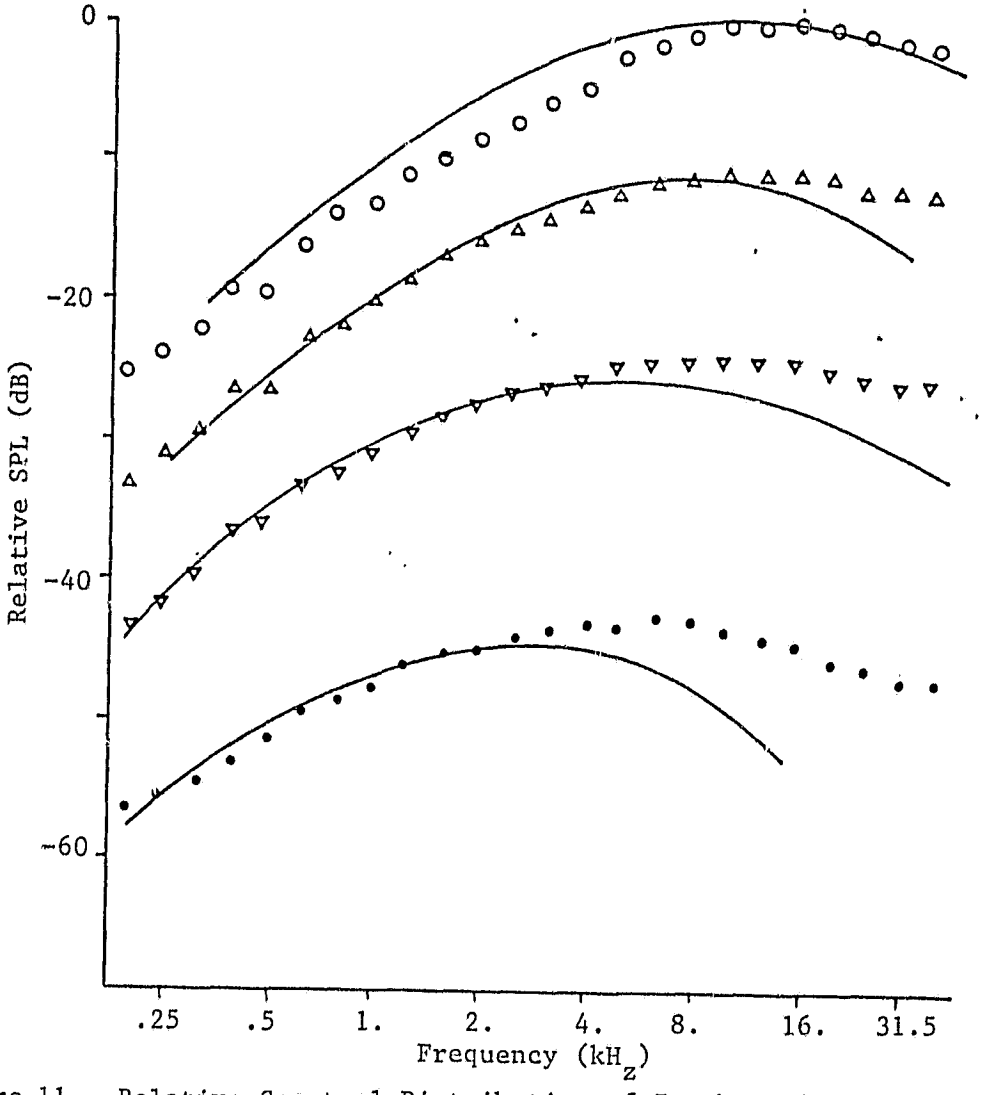

Figure 11. Relative Spectral Distribution of Isothermal Jet Noise at $\beta = 0^{o}$.

O - U_j/c_o = 1.95, Δ - U_j/c_o = 1.33, ∇ - U_j/c_o = 0.90

● - U_j/c_o = 0.50, solid lines - estimate

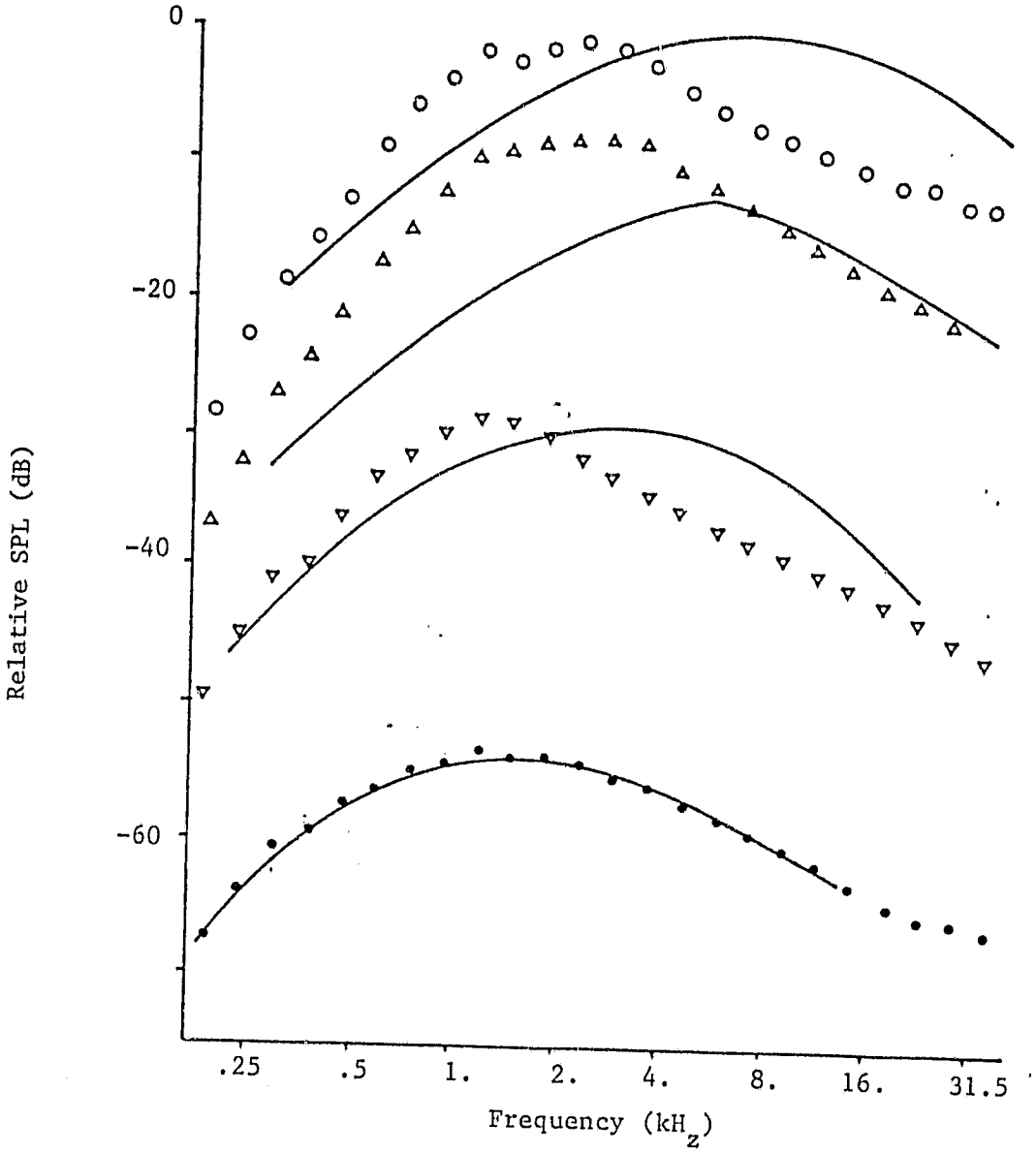

Figure 12. Relative Spectral Distribution of Isothermal Jet Noise at $\beta = 60^{o}$.

O - U_j/c_o = 1.95, Δ - U_j/c_o = 1.33, ∇ - U_j/c_o = 0.90

● - U_j/c_o = 0.50, solid lines - estimate

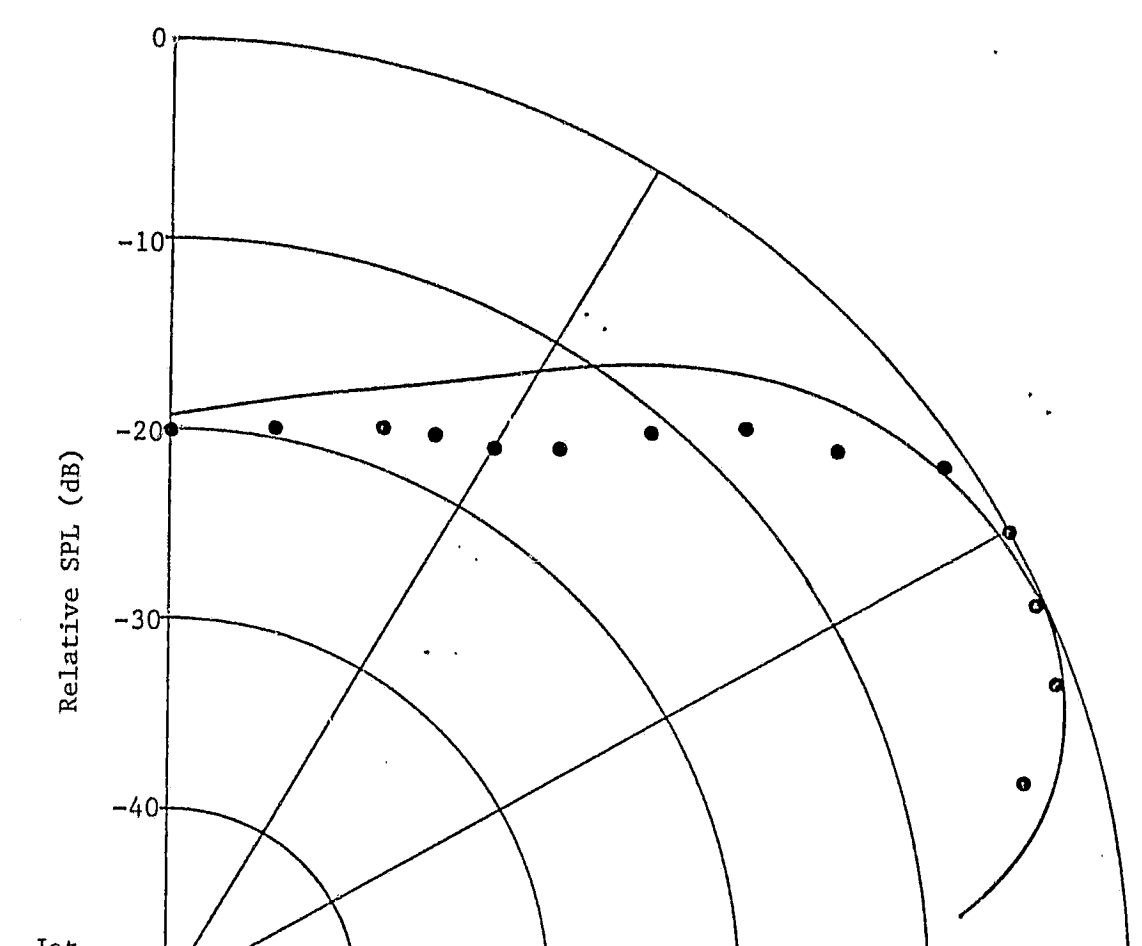

Figure 13. Polar Directivity of Unheated, Supersonic Jet Noise at St = 0.12.

● - measured,

—— - estimate

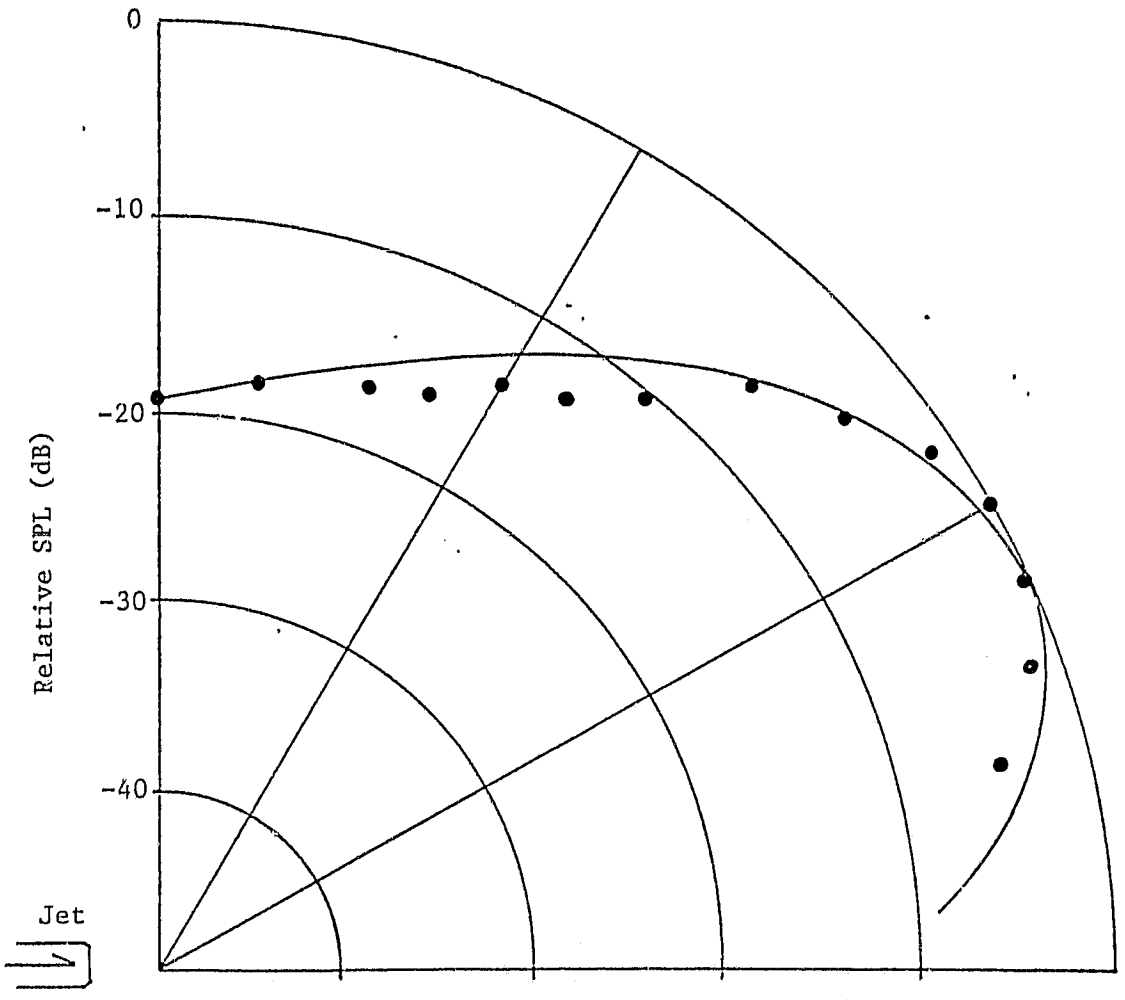

Figure 14. Polar Directivity of Unheated, Supersonic Jet Noise at St = 0.25

● - measured

—— - estimate

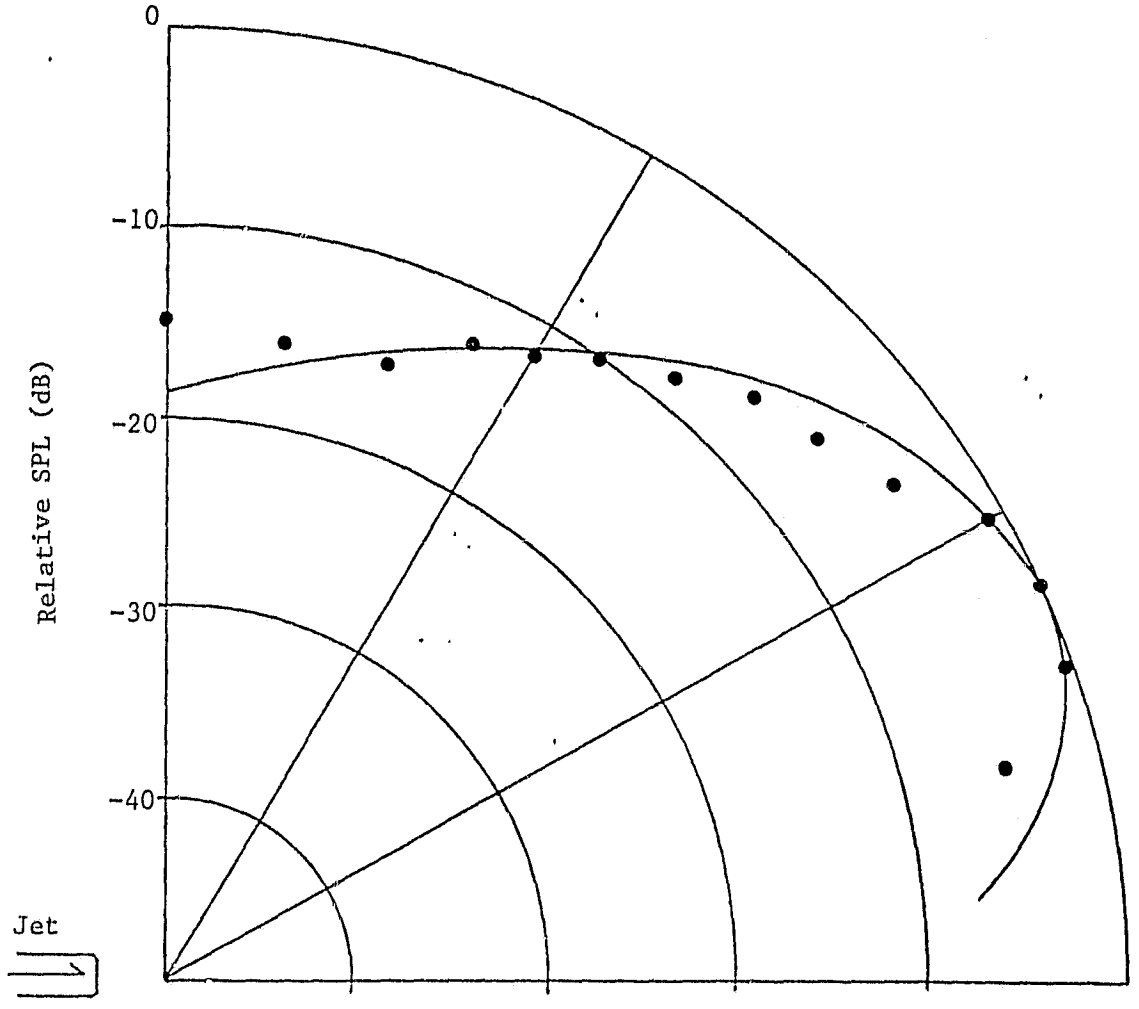

Figure 15. Polar Directivity of Unheated, Supersonic Jet Noise at St = 0.50.

● - measured

—— - estimate

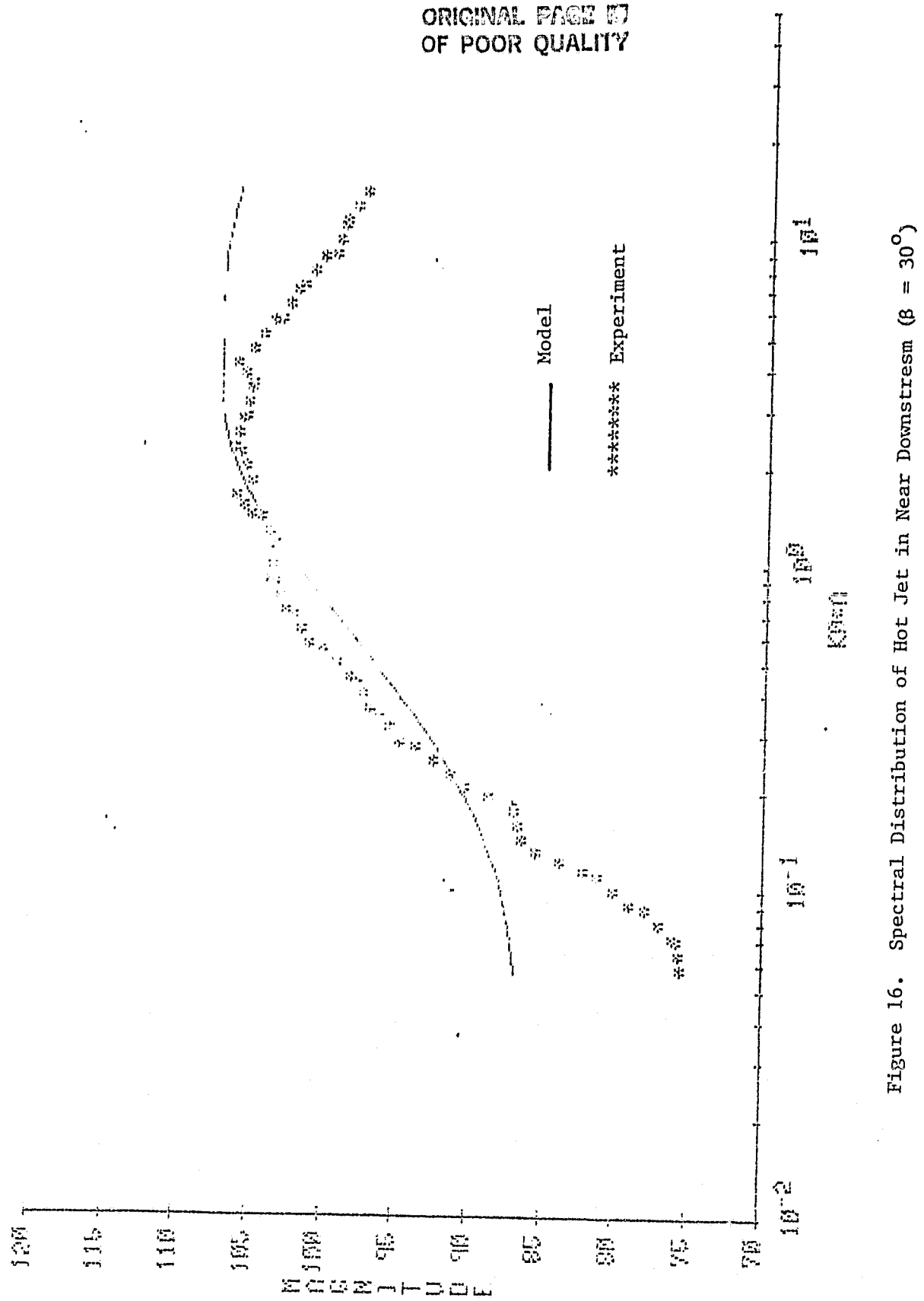

Figure 16. Spectral Distribution of Hot Jet in Near Downstresm ($\beta = 30^{o}$)

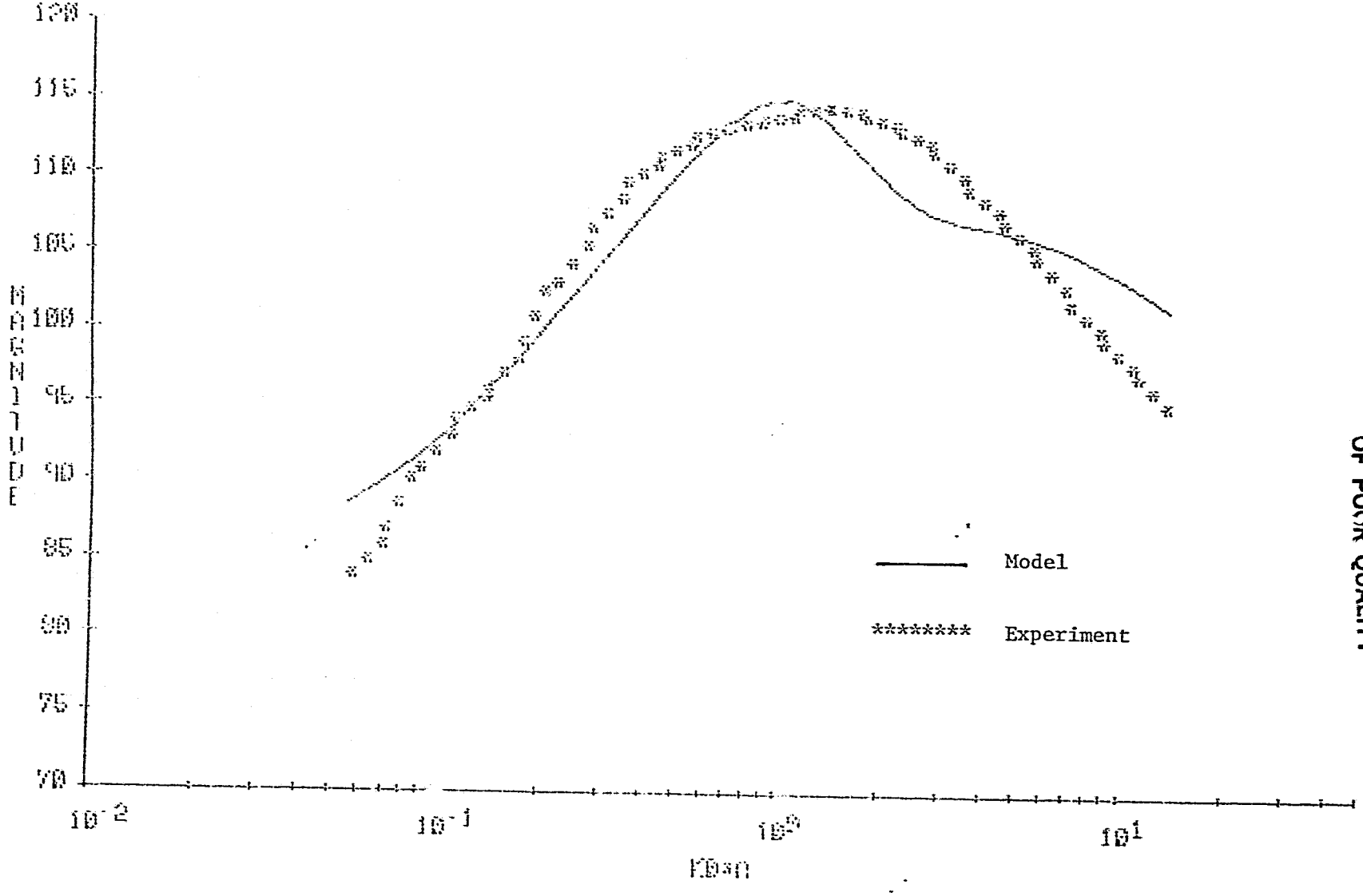

Figure 17. Spectral Distribution of Hot Jet in Far Downstream ($\beta = 60^{o}$)

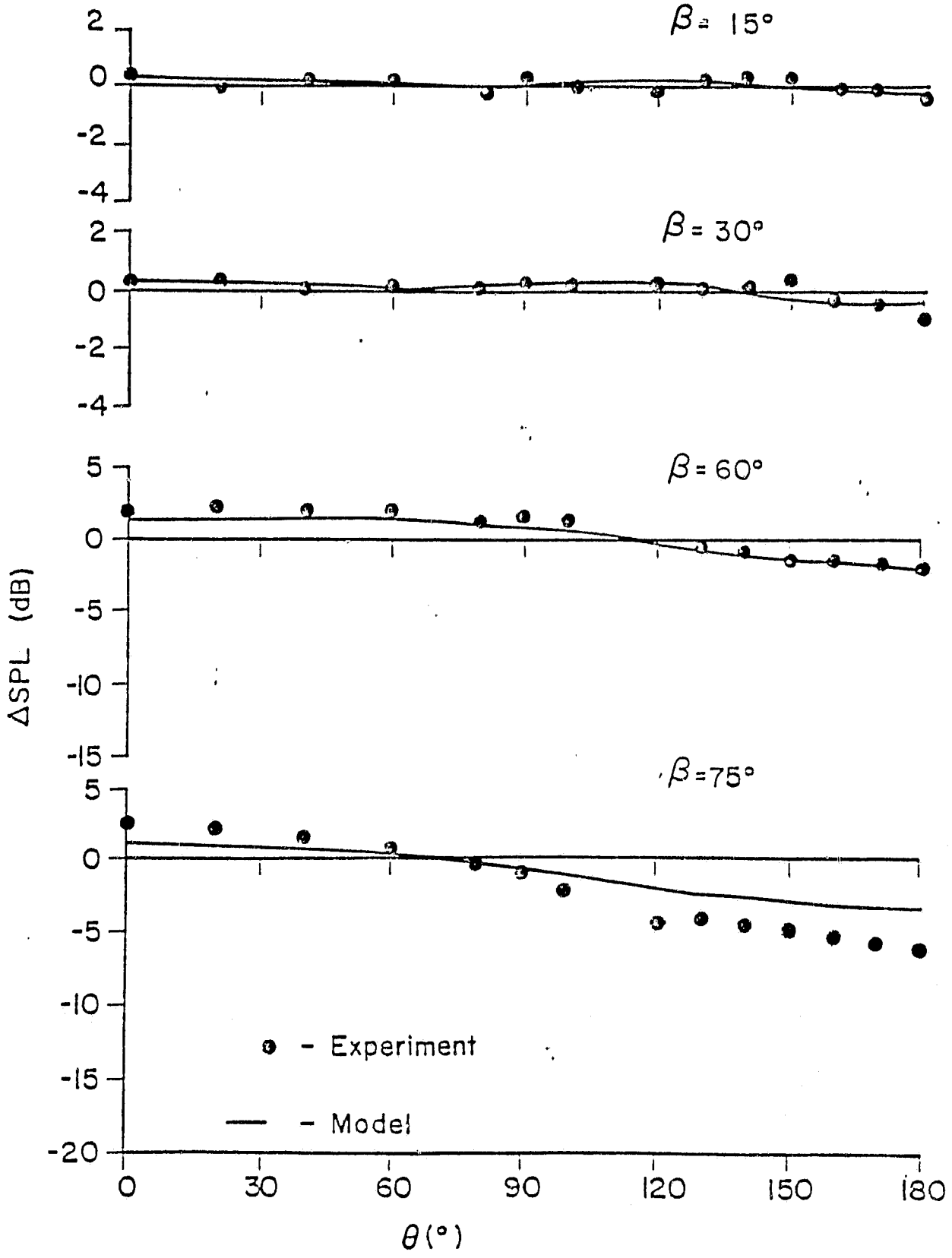

Figure 18. Azimuthal Directivity, Isothermal Jet, M = 0.53, $k_o a$ = 0.56

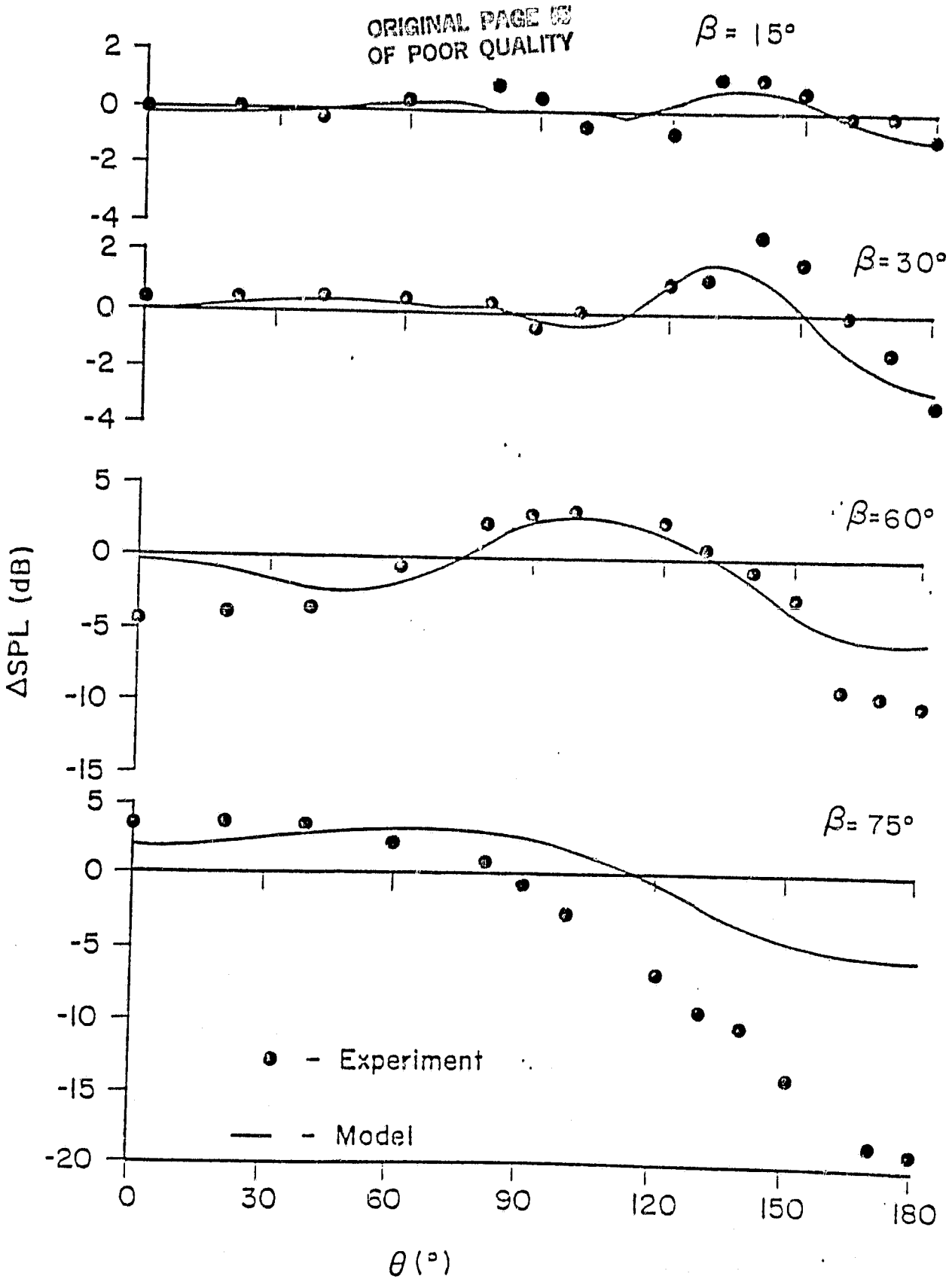

Figure 19. Azimuthal Directivity, Isothermal Jet, M = 0.53, $k_o a$ = 1.6

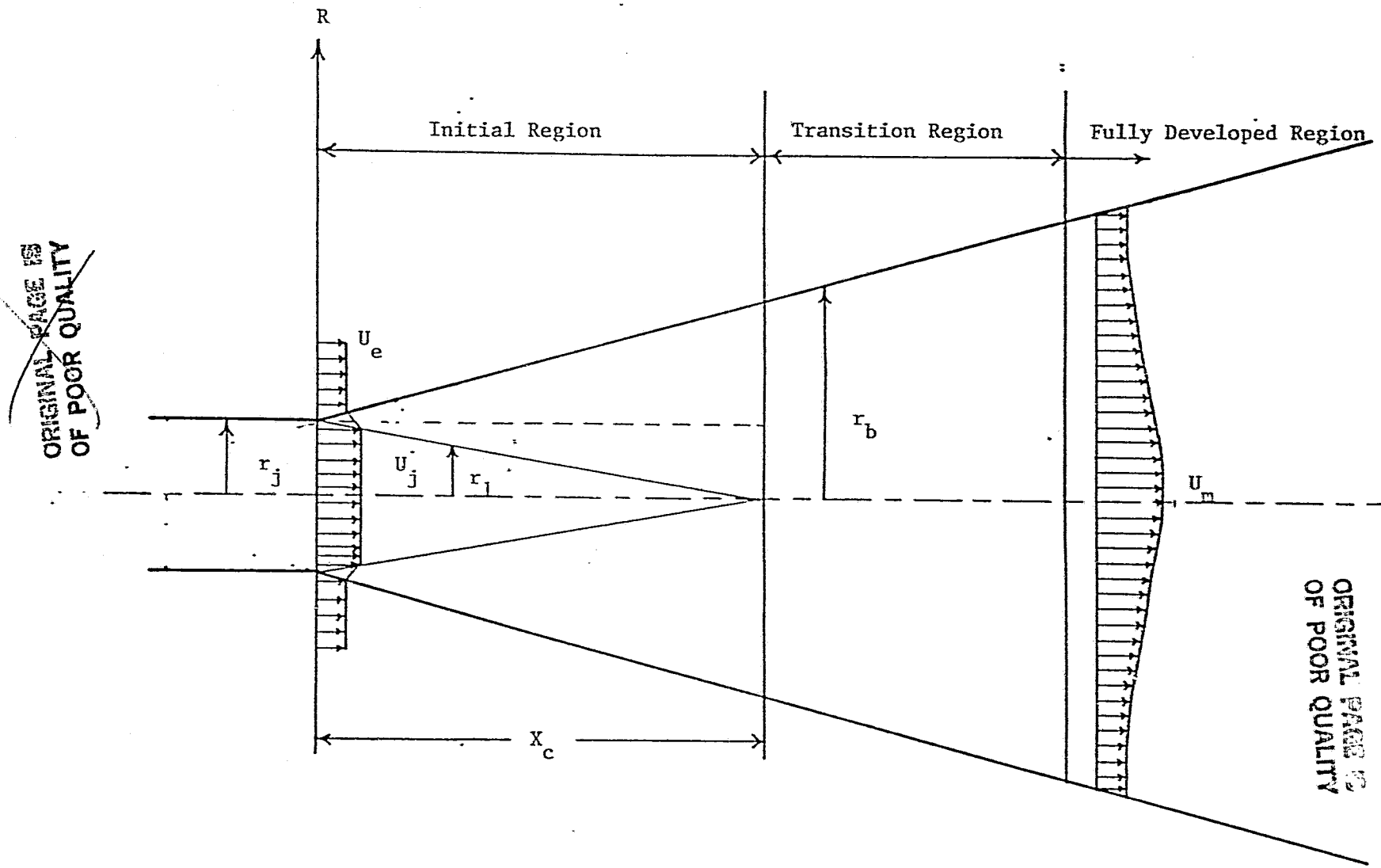

Figure 20. Schematic Representation of Modified Shielding Jet.

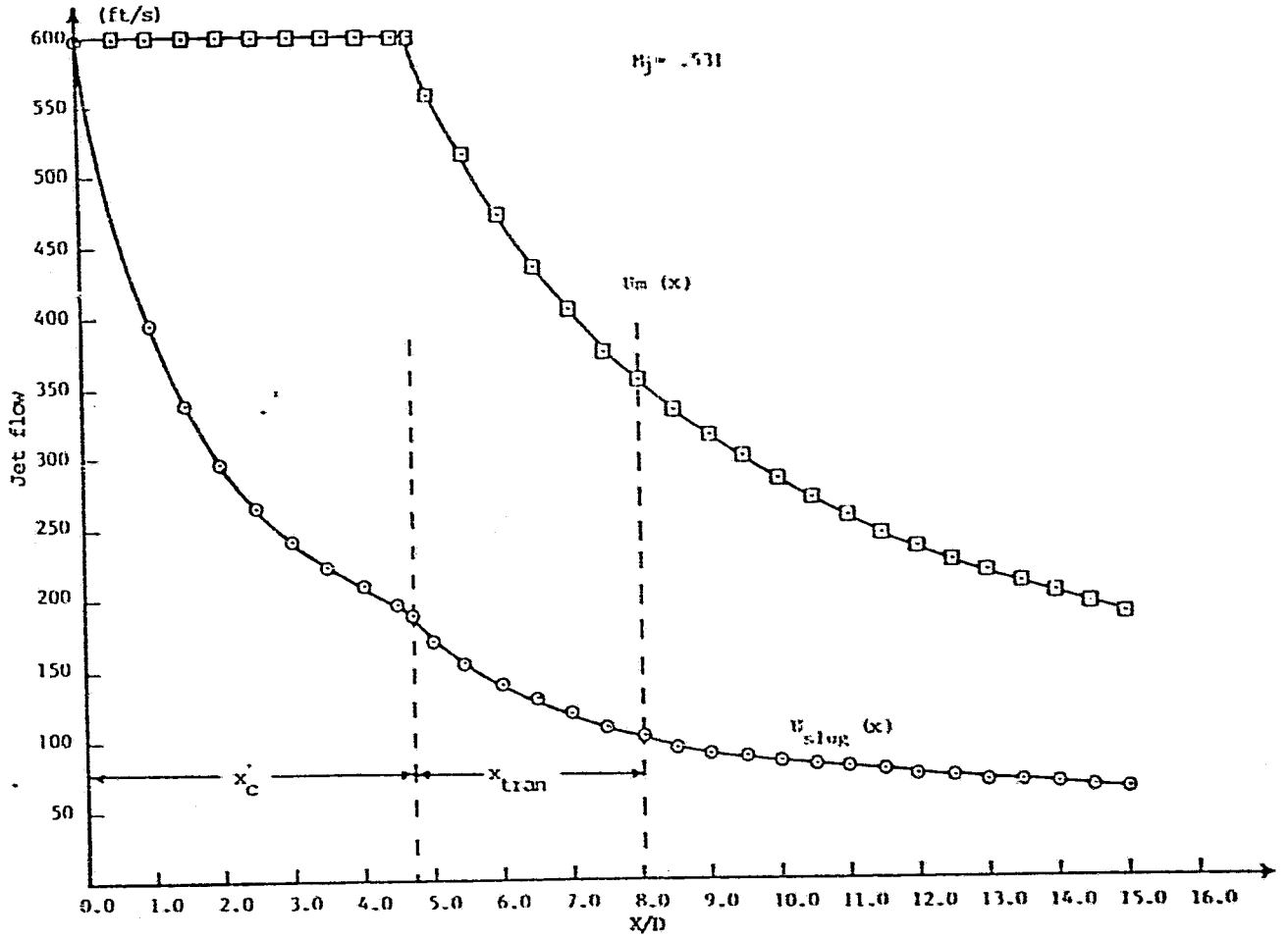

Fig. 21 Downstream centerline and slug flow equivalent velocities

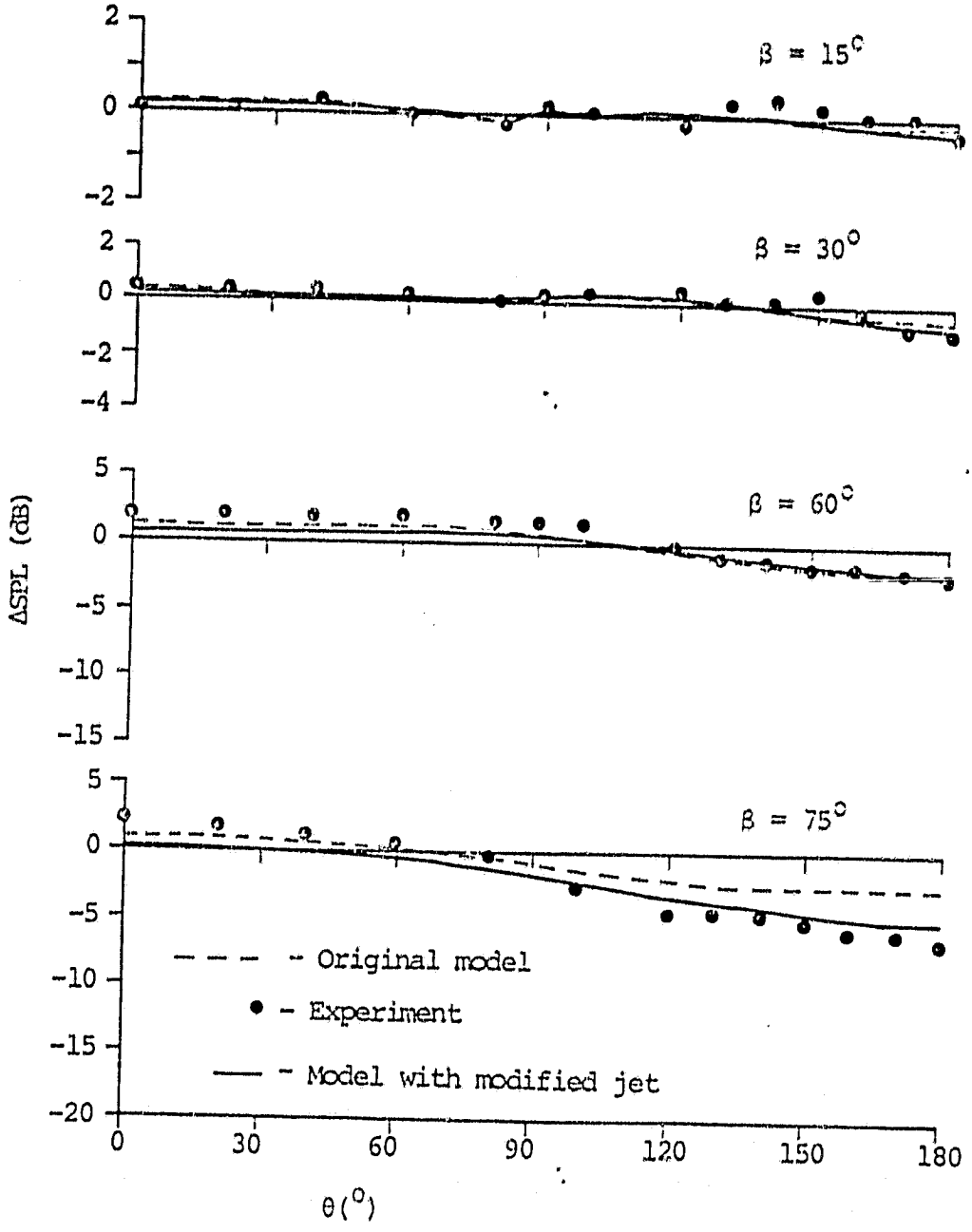

Fig. 22 Azimuthal directivity, modified shielding jet, isothermal jet, M_j = .531, $k_o a$ = .56

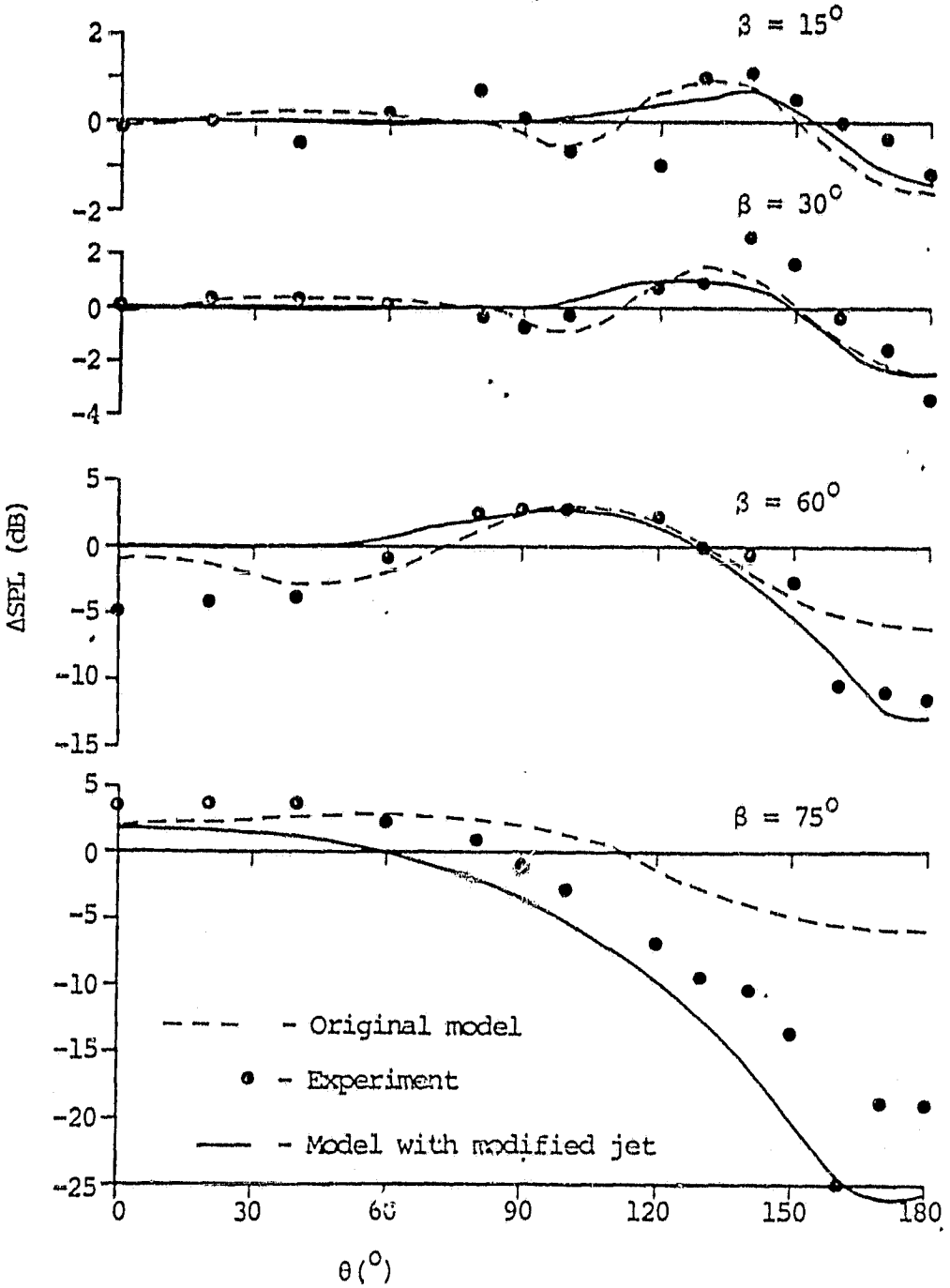

Fig. 23 Azimuthal directivity, modified shielding jet, isothermal jet, $M_j = .531$, $k_0a = 1.6$

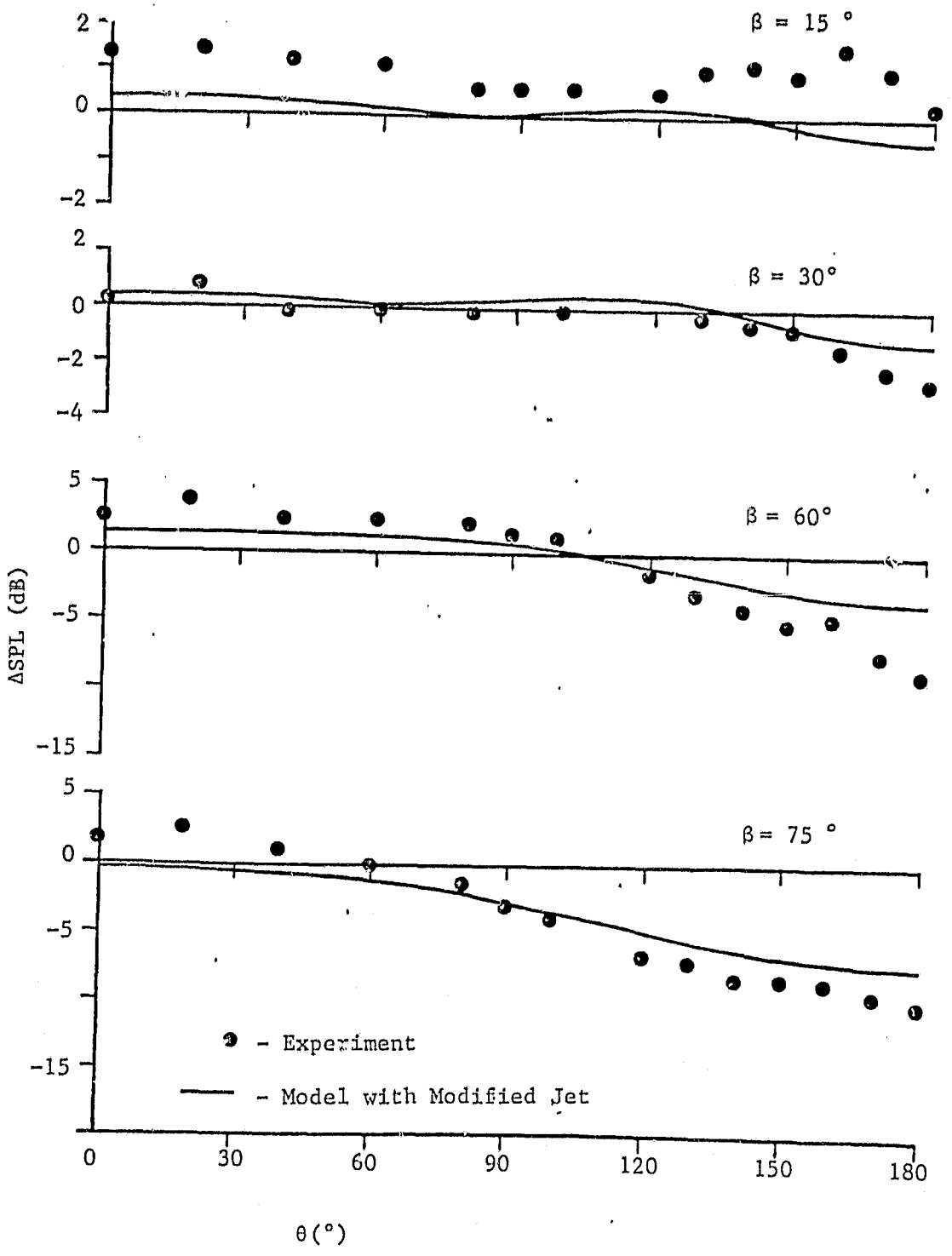

Figure 24. Azimuthal Directivity, Isothermal Jet, M = 0.886, $k_0 a$ = 0.56

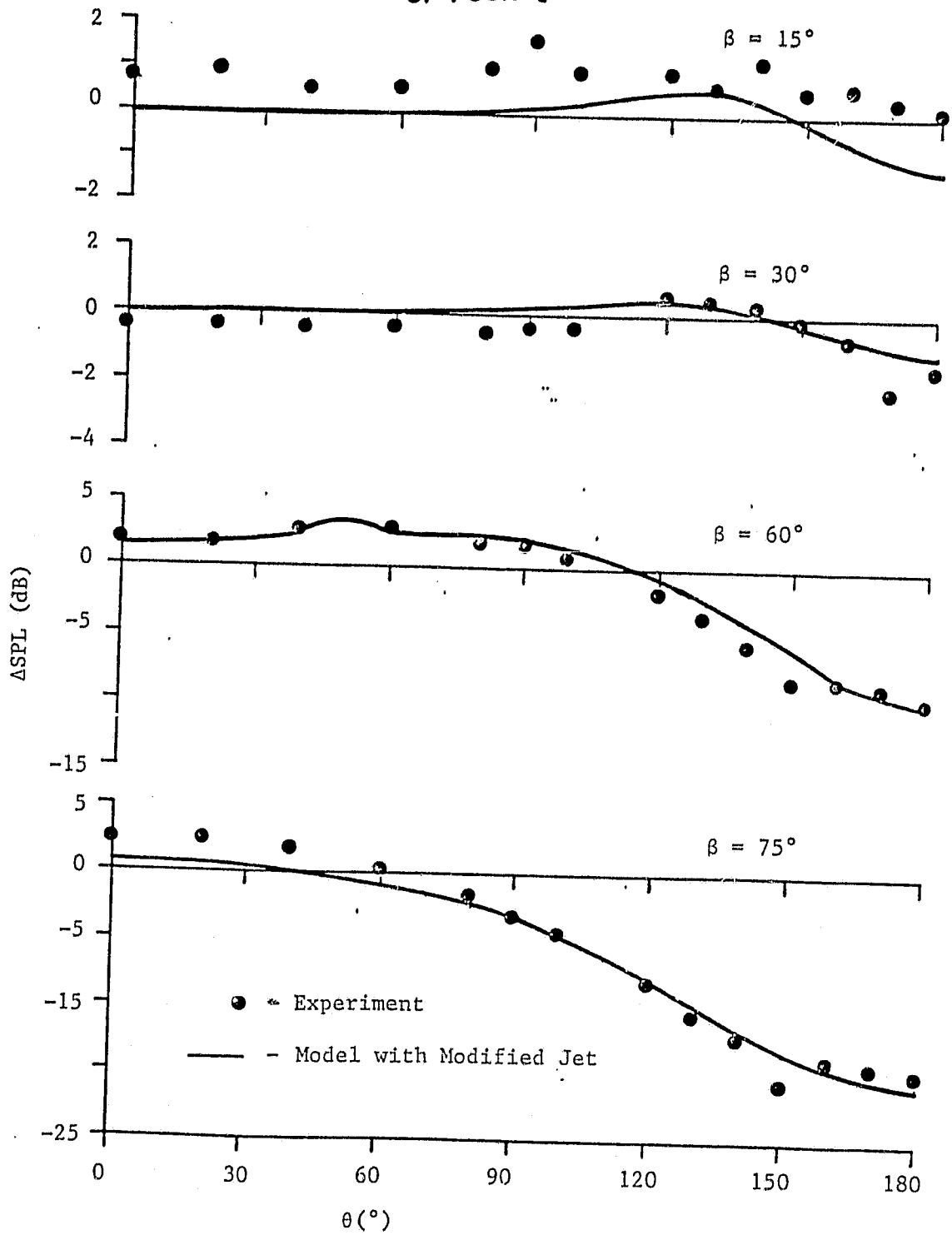

Figure 25. Azimuthal Directivity, Isothermal Jet, M = 0.886, $k_o a$ = 0.96.

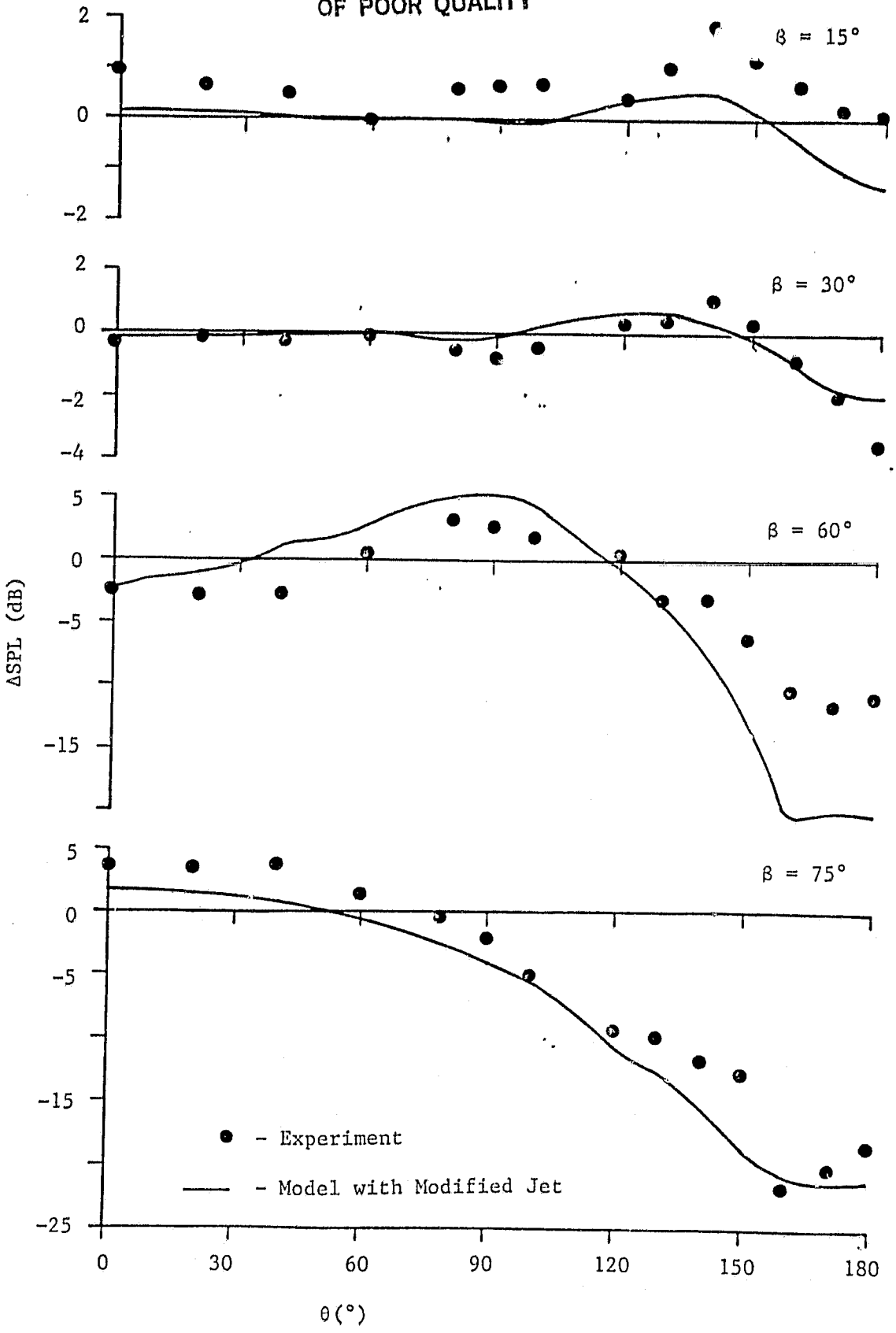

Figure 26. Azimuthal Directivity, Isothermal Jet, M = 0.886, $k_o a$ = 1.6

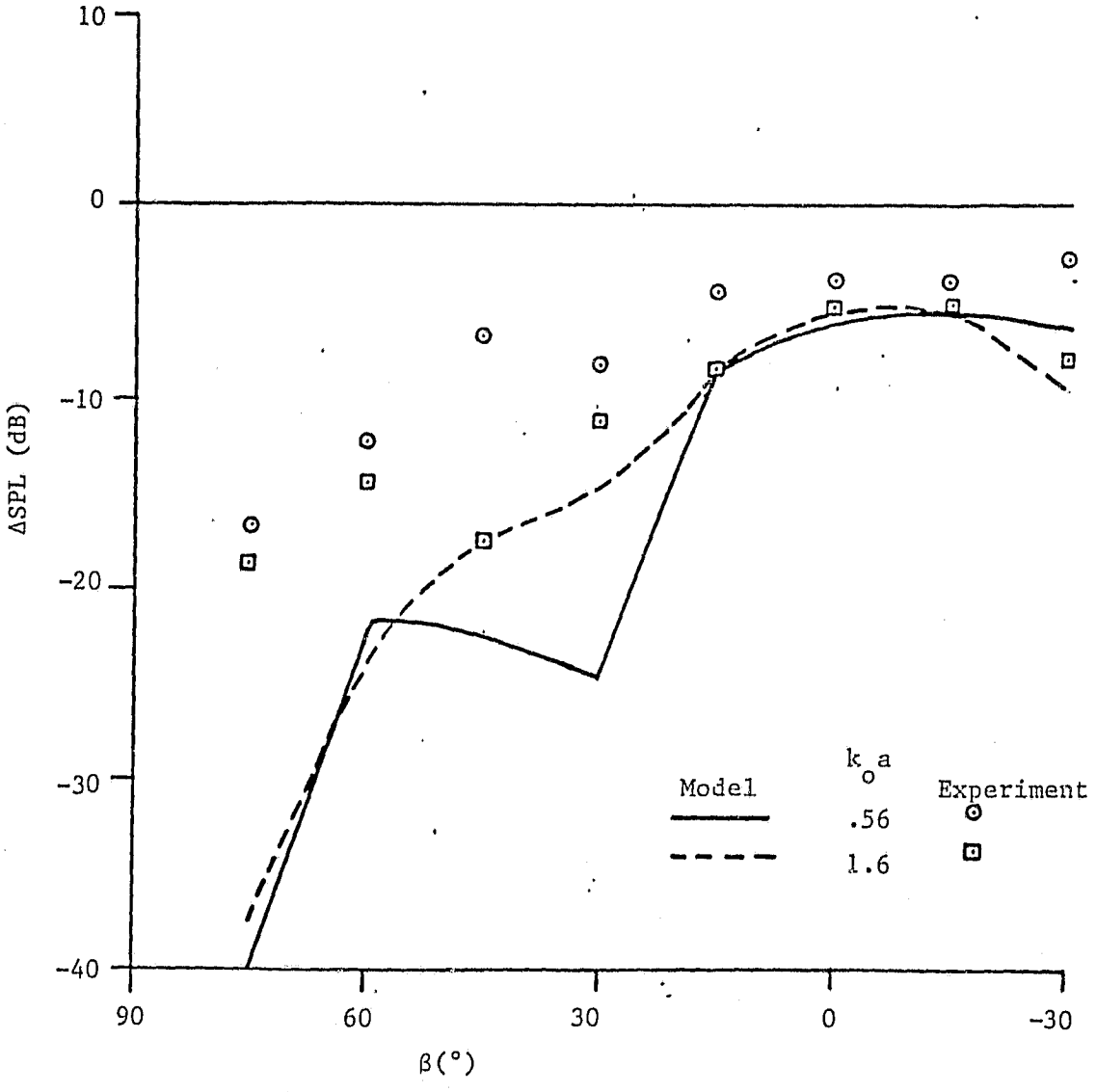

Figure 27. Polar Directivity, Modified Jet Model, Helium Jet, M = 0.177, θ = 180°

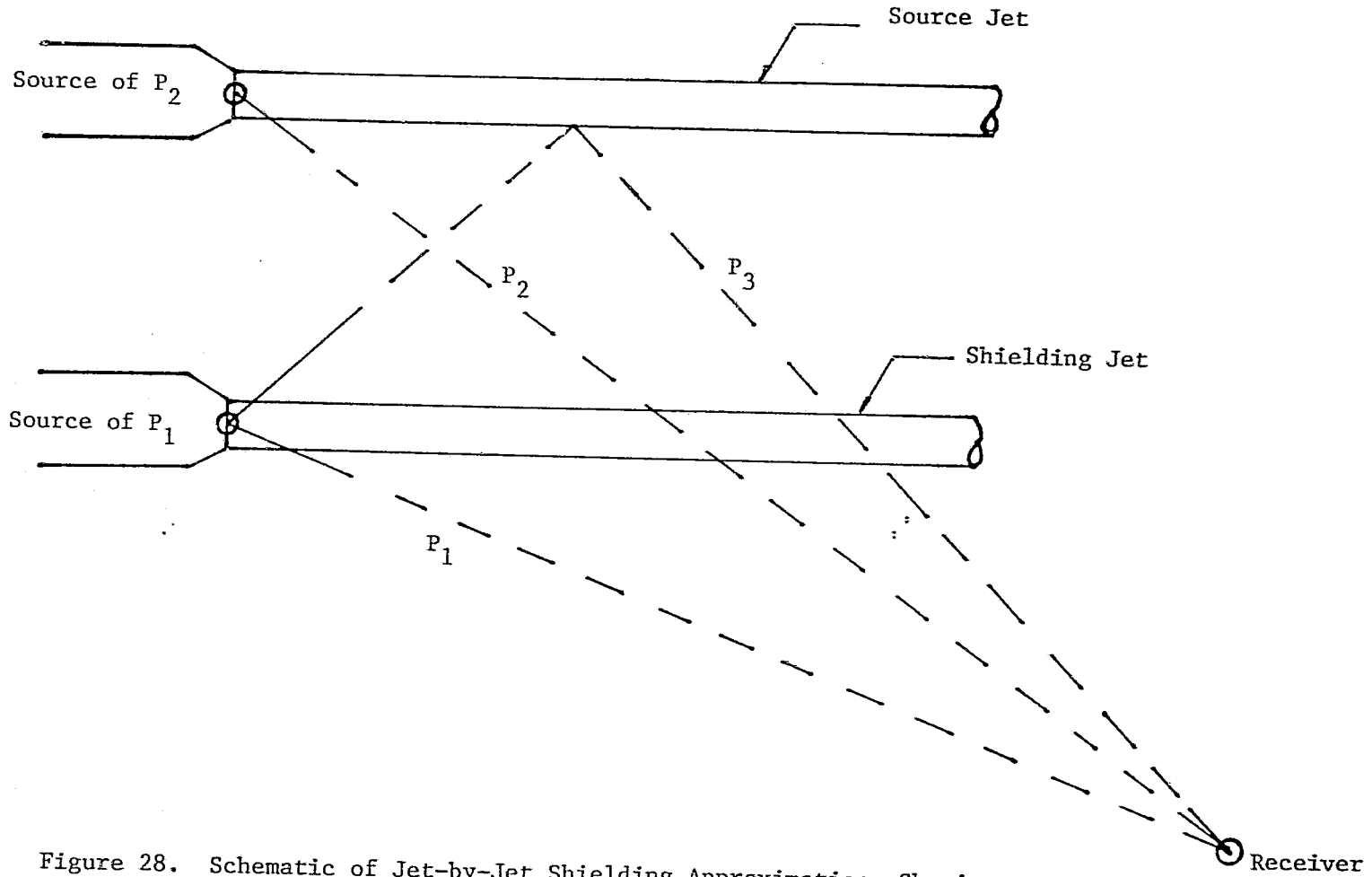

Figure 28. Schematic of Jet-by-Jet Shielding Approximation, Showing Secondary Source due to Reflection of Ray Emitted from Shielding Jet.

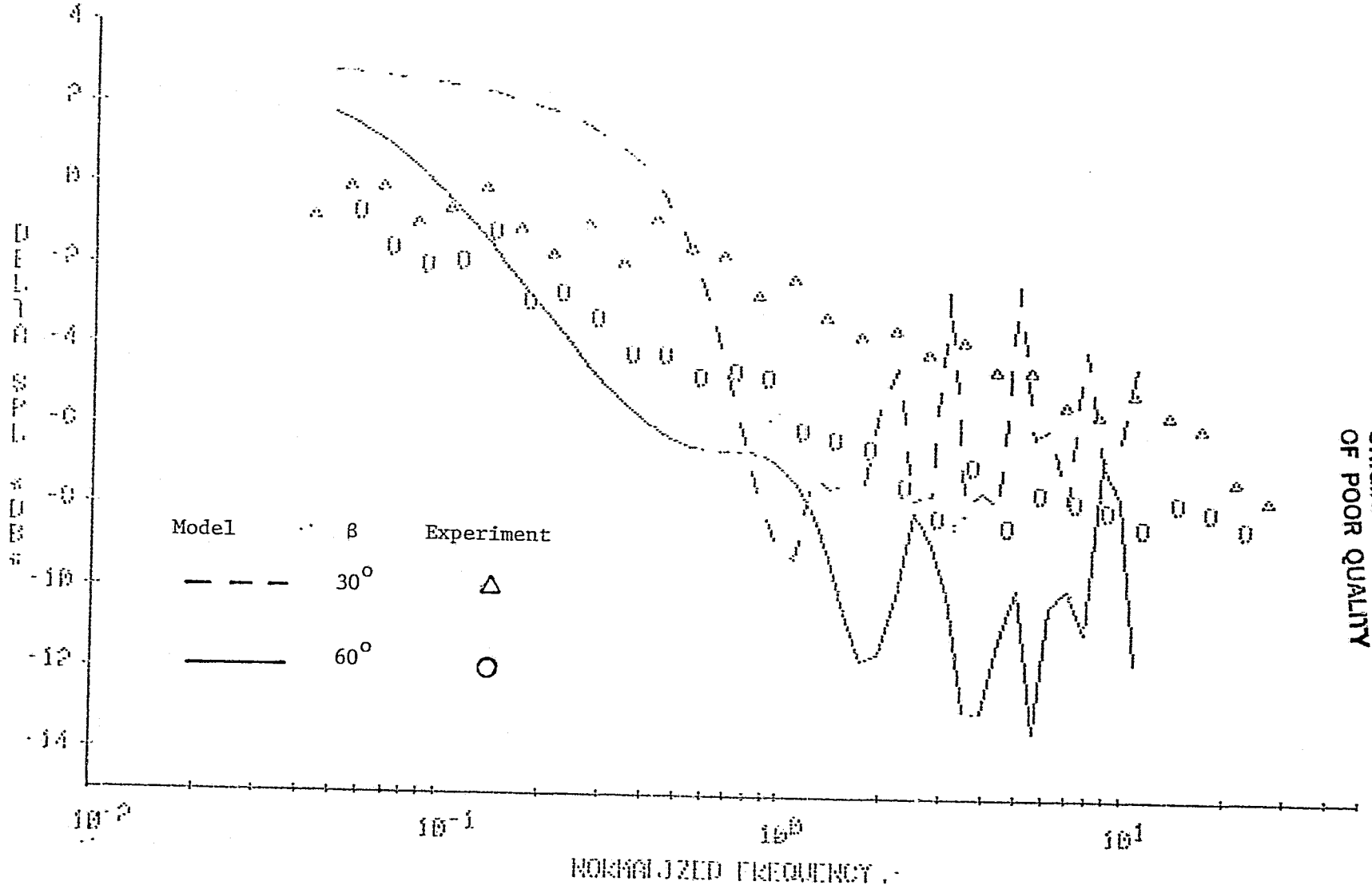

ORIGINAL PAGE IS
OF POOR QUALITY

Figure 29. Attenuation of Jet Noise in Twin-Jet Configuration